Response to comments

Anonymous Referee #1

Received and published: 4 October 2017

This paper discusses the activation of black carbon (BC) containing particles into cloud droplets at a high altitude location. The authors collected cloud-interstitial aerosol (INT), residual aerosol from dried cloud droplets (RES), and aerosol during cloud-free periods. The impact of particle composition and size were then evaluated in regards to the aerosol's ability to activate into a cloud droplet. The largest particles and those with the highest fractions of secondary components, such as sulfate, had the highest activation fractions. However, the relative impacts of these two conditions (size v. composition) on the ability of the particles to be scavenged by the cloud are difficult to distinguish, as the largest particles also contained the highest fractions of secondary components. In addition, two different notations are used to describe the fractions of BC and BC-containing particles in cloud droplets: activation of particles and cloud scavenging. Choosing one of these notations (activation or scavenging) and then evaluating for both number concentrations and BC mass fraction would help streamline the presentation of the results.

We would like to thank the reviewer for his/her useful comments and recommendations to improve the manuscript.

We agree with the comment that the relative impacts of these two conditions (size vs. composition) on the ability of the particles to be scavenged by the cloud are difficult to distinguish. As indicated by the reviewer, larger particles also contained higher fractions of the secondary components. We showed the importance of mixing state through a comparison of the individual particle types of cloud RES with the cloud INT and cloud-free BC-containing particles. As shown in Fig. 5 in the revised manuscript, the number fraction of BC-OC-sul (~8%) was much lower in the cloud RES than those (~25%) in the cloud-free and cloud INT BC-containing particles.

We agree with the comment that choosing one of the notations (activation or scavenging) would help streamline the presentation of the results. We have replaced "activation" to "scavenging" in the revised manuscript, e.g., section 3.2.1 "Size-resolved scavenging of BC-containing particles".

Specific Comments:

Line 163: Of the 7 wavelengths measured, why was 880 nm chosen to use for values of EBC?

Thanks for the comment. At 880 nm wavelength, light absorption can be attributed to BC alone rather than the other aerosol particles due to their significantly less absorption at long wavelength (e.g., Sandradewi et al., 2008; Yang et al., 2009). Therefore, the absorption coefficient at the wavelength of 880 nm is typically chosen to use for the concentration of EBC. We have clarified it in Lines 41-43 of the revised Supplement.

Line 182: For the category of BC-sul1, should this line read "…and less sulfate" or is the sulfate concentration also high for this category? Also, how were the categories determined, i.e. what was the cut-point for categorizing a particle as "more intense sulfate" and "abundance of both sulfate and organics"? Was a specific mass-fraction used to divide the categories?

Thanks for the comment. There was not a specific mass-fraction used to divide the categories. An adaptive resonance theory-based neural network algorithm (ART-2a) (Song et al., 1999) was applied to cluster the individual particles, based on the presence and intensities of ion peaks. The generated particle clusters were further manually grouped. Therefore, the cut-point for categorizing a particle as "more intense sulfate" and "abundance of both sulfate and organics" is based on the intensities (or relative peak area, RPA) of sulfate and organics. To make it clear, we have shown the statistical analysis on the ion peak ratio of OC to BC and the average mass spectra for the BC types, which also shows the relative intensities of sulfate for BC-sul1 and BC-sul2. More intense sulfate (RPA = ~0.3) was found for BC-sul2 and BC-OC-sul, relative to that (RPA = ~0.15) for

BC-sul1 type. More abundance of OC was found for BC-OC-sul, the mean peak area ratio OC/BC of which is ~1, higher than those (< 0.3) for other BC types. Please refer to Fig. S2 in the Supplement.

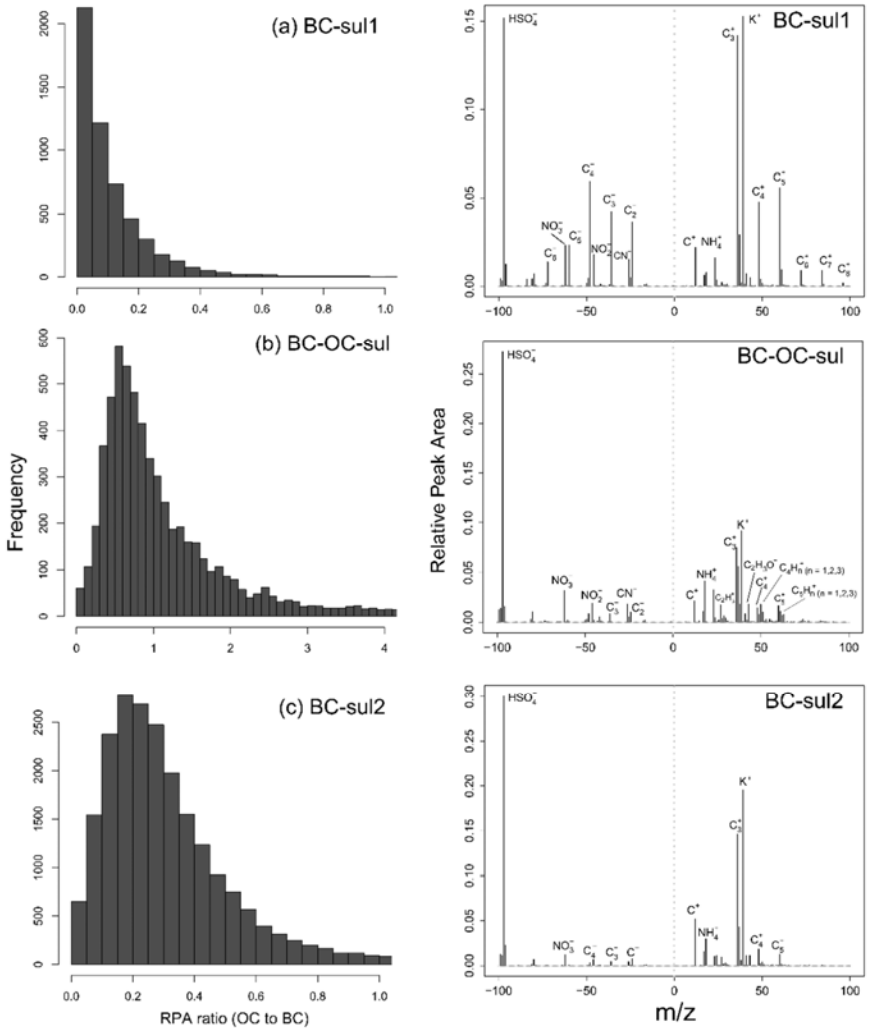

Figure S2. Statistic analysis on the RPA ratio of OC to BC (left), and the average mass spectra (right) for the BC types. Markers were selected as m/z 27, 43, 50, 51, 61, 63, -26 for OC, and carbon ion clusters ($C_n^{+/-}$, $n \leq 5$) for BC, the same as those in Fig. 3. More intense sulfate (RPA = ~0.3) was found for BC-sul2 and BC-OC-sul, relative to that (RPA = ~0.15) for BC-sul1 type. More abundance of OC was found for BC-OC-sul,

the mean peak area ratio OC/BC of which is ~1, higher than those (< 0.3) for other BC types.

Line 204: Is ~0.1% the percentage of BC-containing particles detected only during the 2 hr window or for the whole sampling period for RES?

The ~0.1% here refer to the fraction of cloud RES BC-containing particles during the 2-hour window, when an average temperature was ~ –7 °C. We have revised the sentence to "The cloud RES BC-containing particles only accounted for ~0.1% of all the detected ones in a 2-hour window when the average temperature was ~ –7 °C" to make it clear. Please refer to Lines 211-212 of the revised manuscript.

Line 259: Please clarify what is the meaning of "cannot be ruled out by" in this context and how this relates to the results presented.

Thanks for the comment. To make it clear, we have revised these sentences "An abundance of BC-coated materials was also observed at Mt. Soledad (Schroder et al., 2015). Unfortunately, their chemical compositions cannot be ruled out by a single particle soot photometer. Therefore, our analysis reflects the importance of the chemical mixing state on the cloud processing of BC." to "Although an abundance of BC-coated materials was also observed at Mt. Soledad by a single particle soot photometer (Schroder et al., 2015), the chemical compositions of the coated materials cannot be obtained to provide further information on the mixing state of BC. Our analysis further reflects the importance of the chemical mixing state on the cloud processing of BC."

Line 297: Please clarify how the particles at 700 nm decreased in size to 100 nm for the higher LWC. Is the decrease in size for the diameter of the activated droplets?

Thanks for the comment. It does not mean the decrease in size for the diameter of the activated droplets for the higher LWC. It is the decrease of the half activated diameter for particles to be activated. To avoid the ambiguity, the discussion has been revised to

"Relatively lower scavenging efficiency (0.05–0.45) in the present study was most likely attributed to less dense clouds (with a liquid water content or LWC < 0.1 g m^{-3}). Generally, the half activated diameter increases with decreasing LWC. Henning et al. (2002) stated that particles with d_{ve} = 700 nm were only half activated with LWC < 0.1 g m^{-3}, in contrast, particles with d_{ve} = ~100 nm can be half activated when the LWC > 0.15 g m^{-3}.". Please refer to Lines 319-325 of the revised manuscript.

Line 309: The paragraph starting at line 309 deals solely with the role of mixing state in activation of BC-containing particles. This paragraph would fit more logically in "Section 3.1 Mixing state of BC for cloud-free, residual, and interstitial particles" than in its current location, "Section 3.2.1 – Size-resolved activation of BC-containing particles."

We agree with the comment. The paragraph has been moved to section 3.1 in the revised manuscript, please refer to Line 267-279.

Line 318: The statement that organic-dominated particle types were "activated to a lesser extent" does not seem to be supported by Figure S9. For half of the diameters marked, the organic-dominant particles were nearly equal to or above the activated fraction of BC-containing particles. For the highest 3 diameters marked for the organic-dominant particles, the error bars encompass the range of the BC-containing particles.

Thanks for the comment. We have deleted the statement in the revised manuscript.

Line 322: Is this information (frequency of observation) included in one of the figures (possible figure 3)? If so, please include a reference here to the appropriate figure.

Thanks for the comment. This information is included in Fig. 5. We have clarified it, please refer to Lines 277-279 of the revised manuscript.

Line 370: Was LWC measured in this study? If not, why is the assumption made that the conditions are low-LWC?

LWC was not measured in this study. The LWC in this study was expected to be < 0.1 g m^{-3} according to the discussion in Line 319-325 of the revised manuscript. Generally, the half activated diameter increases with decreasing LWC. Henning et al. (2002) stated that particles with d_{ve} = 700 nm were only half activated with LWC < 0.1 g m^{-3}, in contrast, particles with d_{ve} = ~100 nm can be half activated when the LWC > 0.15 g m^{-3}.

Figure 1: Please add units for the vertical-axis categories. Also, are the PM2.5, EBC, and Num. of BC data for all categories (INT,RES, and cloud-free combined)?

Thanks for the comment. We have revised the Figure 1 accordingly. We have added "$PM_{2.5}$ during the cloud events corresponded to the cloud INT particles. EBC and number of BC-containing particles data were shown for all categories, including the cloud-free, cloud RES, and cloud INT particles. The cloud INT particles were only measured during Cloud III." in the caption of Fig. 1 to clarify the data.

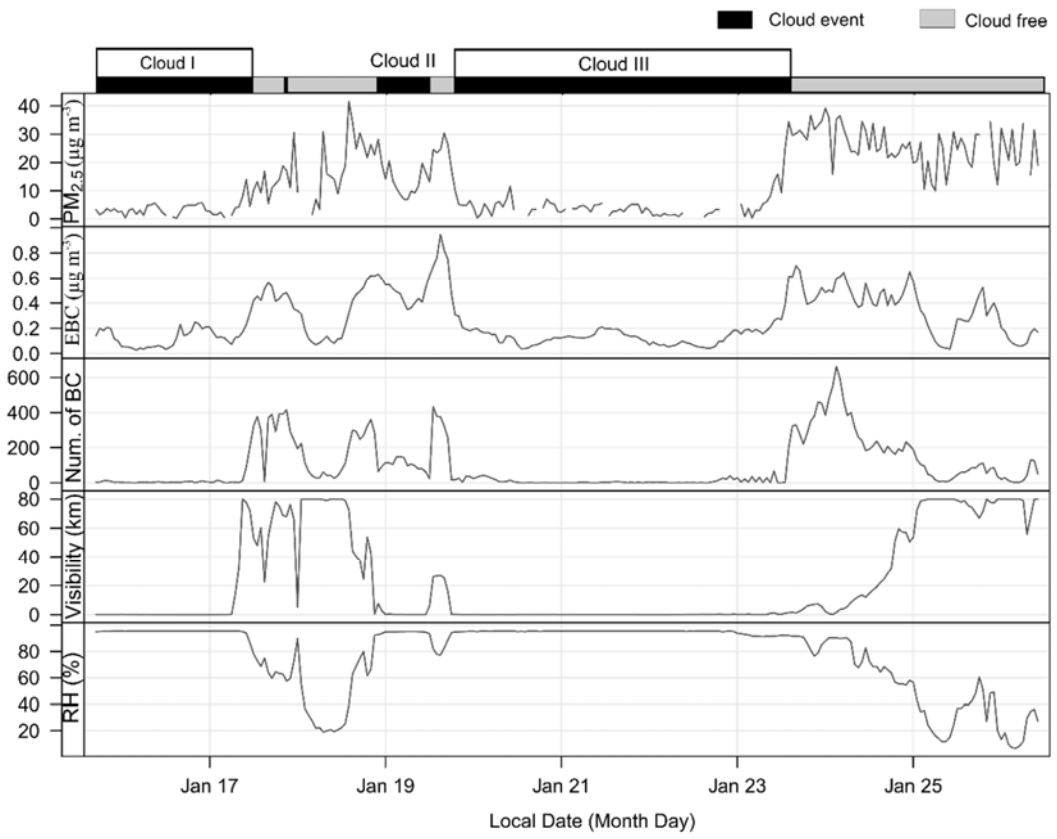

Fig. 1. Temporal profiles (with a 1 hour resolution) of $PM_{2.5}$, EBC mass concentrations, number of BC-containing particles by SPAMS, RH and visibility. Three cloud events are illustrated with black bars above the figure. $PM_{2.5}$ during the cloud events corresponded to the cloud INT particles. EBC and number of BC-containing particles data were shown for all categories, including the cloud-free, cloud RES, and cloud INT particles. The cloud INT particles were only measured during Cloud III.

Supplement Line 59: Please clarify what is meant by "they were taken into account" and how this relates to the calculation of the uncertainties that resulted in 10%.

Thanks for the comment. We have revised to these sentences to "The mean $Mf_{scav,EBC}$ was recalculated to be 30-36%, when the assumed largest underestimate (i.e., 30%) of the cloud RES particles and ~15% underestimate of the cloud INT BC were taken into account in R1. Compared to mean $Mf_{scav,EBC}$ = 33%, the overall uncertainties for the estimate of mean $Mf_{scav,EBC}$ is with 10%." to clarify the statement. Please refer to Lines 65-68 of the revised

Supplement.

Figure S8: Please clarify in the caption the line: "the other particles also contained OC particles (10%)." Does 10% refer to the percent of total particles containing any amount of OC or the percent of total particles that had OC as the dominant species?

Thanks for the comment. We have clarify that 10% refer to the percent of total particles had OC as the dominant species. Please refer to Line 128 of the revised Supplement.

Technical Corrections:
Lines 336-337: Please divide these lines into two sentences: "...areas (Huang et al., 2012). It is similar to those..."

Thanks for the suggestion. It has been revised as suggested.

Response to comments

Anonymous Referee #2

Received and published: 22 October 2017

This paper presents aerosol particle mixing state measurements and analysis of black carbon containing cloud drop residuals obtained during a 10 day campaign from a ground station at a remote mountain site located in southern China. Cloud droplet residual particles were sampled with a ground based CVI operating behind a compact wind tunnel and analyzed with a SP-AMS, SMPS, and an aethalometer. Drivers for activation, including residual composition and particle size, are investigated. Results are compared with concurrent cloud-free and interstitial aerosol particle sampling.

General comments:
This paper seems to be portrayed as an in-depth study on particle mixing state and the influence of mixing state and anthropogenic activities on CCN activity; however, it may be more accurately described as an individual case study, looking at three cloud events in a single location. Care should be taken not to over-emphasize the implications of these results to all aspects of cloud activation processes. Support qualitative statements throughout the paper with quantitative results.

We would like to thank the reviewer for his/her useful comments and recommendations to improve the manuscript.

We agree with the comment that it is more accurately described as an individual case study. We have revised the title to "The single-particle mixing state and cloud scavenging of black carbon: a case study at a high-altitude mountain site in southern

China". We also attempt to support qualitative statements throughout the paper with quantitative or semi-quantitative results as suggested. Please refer to the response to the specific comments as follows.

Specific comments:

Line 23-24: Other references have looked at the mixing state of BC particles in China. (e.g., Cheng et al. 2006; Wang et al., 2014). You have also referenced mixing state measurements by Huang et al. (2011) in Figure S7. You also reference another report of scavenging of BC particles made in China (Lines 70-72; Zhou et al., 2009)

We agree with the comment that mixing state and scavenging of BC particles have been previously investigated in China. In this study, we first attempted to link the cloud scavenging efficiency of BC particles directly with their mixing state in China. We thus revised the sentence to "In situ investigation on the cloud scavenging of BC in company with the mixing state was first reported in China" to make it clear. Please refer to Lines 23-24 of the revised manuscript.

Line 25-26: Please clarify or quantify the use of 'same extent'. Are you saying that the number fraction of particles containing black carbon is the same between 'cloud RES', 'cloud INT', and 'cloud free'?

Thanks for the comment. We have revised the sentence to "The number fraction of scavenged BC-containing particles is close to that of all the measured particles."

Line 27-28: This statement seems to contradict the previous (Line 25-26).

Thanks for the comment. As we discussed in Supplement Lines 126-128, it is attributed to two reasons: (1) BC-OC-sul particles only accounted for ~20% of BC-containing

particles, and (2) the other particles also contained OC-dominated particles (~10%).

Line 46: A number of studies have previously reported black carbon measurements in the free troposphere (e.g., Schwarz et al., 2013; Pusechel et al., 1992; Pósfai et al., 1999; Babu et al., 2011; Liu et al., 2010)

We agree with the comment that several studies have previously reported black carbon measurements in the free troposphere. However, simultaneous measurements on the mixing state and cloud scavenging of BC are still rare. We have revised the sentence to "Our results would improve the knowledge on the concentration, mixing state, and cloud scavenging of BC in the free troposphere." to clarify the statement.

Line 48: Please expand on the usability of these results in modeling studies.

Thanks for the comment. Our results on the concentration and cloud scavenging of BC could be used as a reference to compare with the modeling results, with respect to the southern China. As stated in the previous response, we have revised the sentence to "Our results would improve the knowledge on the concentration, mixing state, and cloud scavenging of BC in the free troposphere." to clarify the statement.

Line 50: Change 'residues' to 'residuals' for consistency.

It has been revised to "residual particles" accordingly.

Line 55: Fresh soot particles are generally very hydrophobic and generate organic layers over time, decreasing their hydrophobicity. Per your reference: "While freshly emitted soot is extremely hydrophobic, oxidation during aging causes soot to become more hydrophilic." (Zuberi et al., 2005)

Thanks for the comment. We have corrected “hydrophilic” to “hydrophobic”, and thus sentence was revised to “Fresh BC-containing particles are generally hydrophobic due to the presence of thin coatings of inorganic or organic materials (Zuberi et al., 2005), and during transport they become more hydrophilic when further coated through coagulation, condensation and photochemical oxidation (Zuberi et al., 2005; Zaveri et al., 2010; Matsui, 2016).”.

Line 60-61: This seems to contradict your statement in the abstract that “…measured BC-containing particles… were activated into cloud droplets to the same extent as all the measured particles”

Thanks for the comment. As we stated in the above response, freshly emitted BC particles are extremely hydrophobic, atmospheric aging (e.g., through coagulation, condensation and photochemical oxidation) causes them to become more hydrophilic. The in-cloud scavenging of BC should be enhanced to some extent, may be to the same extent as other aerosol compositions. Therefore, it does not contradict the statement in the abstract.

Line 72: Change ‘residues’ to ‘residuals’ for consistency.

It has been revised to “residual particles” accordingly.

Line 74: Change ‘would be altered’ to ‘could be altered’.

It has been changed as suggested.

Line 90: Change ‘residues’ to ‘residuals’ for consistency.

It has been revised to “residual particles” accordingly.

Line 112-116: What is the average boundary layer height compared to the surrounding ground altitude for this region? How frequently is this site sampling free tropospheric air?

Thanks for the comment. The average boundary layer height over the study compared to the surrounding ground altitude for this region is ~280 m, with the highest boundary layer height at ~1000 m. Regarding that the average surrounding ground altitude is ~500 m, it is reasonable to consider this site sampling free tropospheric air throughout the study. It is noted the boundary layer height was not measured over the study, instead, it is calculated from https://www.arl.noaa.gov. This information has been added in the revised manuscript, please refer to Lines 116-119.

Line 115: Change ‘isolated’ to ‘distant’ (indicate that it is not near any anthropogenic sources).

It has been changed as suggested.

Line 120: What is the particle size transmission efficiency for this wind tunnel set up? Are larger droplets transmitted through the tunnel with the same efficiency as smaller droplets?

Generally, the transmission efficiency of the droplets increased with increasing size, with 50% transmission efficiency at 8 μm. The detail information on the design and testing on the size-resolved transmission efficiency of the CVI inlet can be available elsewhere (Shingler et al., 2012). The inlet cut size was set to be 8 μm, at which the

transmission efficiency of droplets is 50%. This information has been added in the sampling setup, please refer to Lines 126-129 of the revised manuscript.

Line 121: What is the wind tunnel velocity used for the ground based setup? Was it ~80 m/s? You've reported an enhancement factor of 5.25 (Line 138), which would require a free stream velocity of ~80 m/s at 15 LPM sample flow in the BMI CVI.

The wind tunnel velocity used in this study is ~80 m/s. As suggested by the reviewer in the following comments, we have added this information in the revised manuscript as "A_{tip} is 1.67×10^{-5} m^2, q_{sample} is 15 l min^{-1}, and V_{air} was set to be ~80 m/s, coincides with an EF of 5.25.", please refer to Lines 129-133.

Line 127: Change "...particles that are capable of acting as CCN" to "...particles that were CCN"

It has been changed as suggested.

Line 127-128: Please clarify what you mean by "A testing before measurements demonstrates that the influence of background aerosols on the collection of cloud droplets could be negligible..."

Thanks for the comment. To make it clear, we have changed the sentence to "The influence of background particles on the collection of the cloud RES particles could be negligible. A test on the cloud-free air showed that the average particles number concentration sampled by the GCVI was ~1 cm^{-3}, far below the level ~2000 cm^{-3} in the cloud free air over the study (Zhang et al., 2017).".

Line 133-136: Please provide further information on the GCVI measurement

capabilities (visibility and rainfall detection). How are these measured by the instrument?

Thanks for the comment. We have added "The GCVI includes various sensors to monitor the temperature/RH, visibility (http://belfortinstrument.com/products/all-environment-visibility-sensor/), and rainfall/snow (http://www.meltyourice.com/products/controllers/ds-82/). The integrated rainfall/snow sensor helps to exclude sampling during rainy periods." in the Supplement, please refer to Lines 78-82.

*Line 137-139: Please change the following: "The enhancement factor (EF) for the particles collected by the GCVI is 5.25 (Shingler et al., 2012)" to indicate that the enhancement factor (EF) for the particles collected by the GCVI is calculated as EF = Atip*Vair/qsample, where this results in an EF for your setup of 5.25 using your wind tunnel velocity and your sample flow rate.*

We agree with the comment. We have changed these sentences to "The enhancement factor (EF) was calculated according to the equation (Shingler et al., 2012): EF = A_{tip}*V_{air}/q_{sample}, where A_{tip} is the area of the inlet tip where drops enter, V_{air} is wind tunnel velocity, and q_{sample} is the volumetric flow rate of sampled air in the CVI inlet. A_{tip} is 1.67×10^{-5} m^2, q_{sample} is 15 l min^{-1}, and V_{air} was set to be ~80 m/s, coincides with an EF of 5.25." in Lines 129-133 of the revised manuscript.

Line 140-149: Please provide uncertainties and detection limits for your instrument measurements or references for where this information can be found (state that this information is in the supporting information if necessary). Please provide total size range and bin resolution information for the SMPS instruments.

Thanks for the comment. The information on the uncertainties and detection limits of

our instrument measurements has been added in the Supplement as suggested. We also provided the information on the total size range and bin resolution for the SMPS instruments.

The detection limit for EBC measurements is < 10 ng m^{-3} with uncertainty at ~2 ng m^{-3} at the time-base of 1 minute. TEOM (https://www.thermofisher.com) measures the mass concentration of aerosol with the detection limited of ~100 ng m^{-3}, with an accuracy of ±0.75%. MSP SMPS (https://www.mspcorp.com) measures the number-based size distribution of particles ranged between 10-1000 nm in 48 size bins, with a detection limit of ~1 cm^{-3}, and an accuracy of ±10%. Grimm SMPS (https://www.mspcorp.com) measures the number-based size distribution of particles ranged between 10-1100 nm in 44 size bins, with a detection limit of ~1 cm^{-3}, and an accuracy of ±5%. The accuracy for the particle size measured by the SPAMS is within ±10%. Please refer to Lines 31, 55-57, and 82-89 of the revised Supplement.

Line 143: Change 'scan' to 'scanning'.

It has been changed as suggested.

Line 163: What MAC values were used to convert to EBC concentrations?

We have added the MAC values and the corresponding references for where the values are suggested. The sentence has been revised to "For AE–31, a specific attenuation cross-section σ_{ATN} of 16.6 m^2 g^{-1}, recommended by the manufacturer, was applied to calculate the EBC concentration with the equation: EBC = b_{ATN}/σ_{ATN}, where b_{ATN} is the optical attenuation coefficient. For AE-33, the ATN was converted to an EBC concentration using the mass absorption cross section of 7.77 m^2 g^{-1} according to the method recommended by Drinovec et al. (2015).". Please refer to Lines 44-48 of the revised Supplement.

Line 213: Change 'approximate' to 'approximately'.

It has been changed as suggested.

Line 216-218: This is a single event (Cloud II) and more sampling should be conducted to support this claim.

We agree with the comment. The mass concentration of EBC during Cloud II was approximately 200 ng m^{-3}, which is four times that (~50 ng m^{-3}) observed during the other two events. It is attributable to the strong impact of the northeastern air mass (Lin et al., 2017). We have clarified that this is a case study in the revised manuscript and revised the statement to "This case might provide partial evidence for the influence of anthropogenic emissions and atmospheric transport on the formation of clouds at the remote high-altitude site in southern China.", please refer to Line 222-224 of the revised manuscript.

Line 225-227: Do these percentages indicate the number of total particles that had detectable amounts of these individual components?

Thanks for the comment. These percentages indicate the number of total particles that had detectable amounts of these individual components. We have added "Y-axis indicates the number fraction of total particles that had detectable amounts of these individual ion peaks." to Fig. S3 to make it clear.

Line 247-261: There are many qualitative statements in this section that would benefit from supporting quantitative results (e.g., "…the enhancement was more obvious...", "…particles have been broadly observed…", "An abundance of BC-coated

materials…", etc..)

We agree with the comment. An adaptive resonance theory-based neural network algorithm (ART-2a) (Song et al., 1999) was applied to cluster the individual particles, based on the presence and intensities of ion peaks. The generated particle clusters were further manually grouped and three BC particle types were obtained. Therefore, the cut-point for categorizing a particle as "more intense sulfate" and "abundance of both sulfate and organics" is based on the intensities of sulfate and organics. To make it clear, we have shown the statistical analysis on the ion peak ratio of OC to BC and the average mass spectra for the BC types. More intense sulfate (RPA = ~0.3) was found for BC-sul2 and BC-OC-sul, relative to that (RPA = ~0.15) for BC-sul1 type. More abundance of OC was found for BC-OC-sul, the mean peak area ratio OC/BC of which is ~1, higher than those (< 0.3) for other BC types. Please refer to revised Fig. S2.

Line 259-260: Please explain this sentence, or link it to the previous study.

Thanks for the comment. This sentence has been revised to "Although an abundance of BC-coated materials was also observed at Mt. Soledad by a single particle soot photometer (Schroder et al., 2015), the chemical compositions of the coated materials cannot be obtained to provide further information on the mixing state of BC." to make it clear, as also commented by the Referee 1#. Please refer to Lines 262-266 of the revised manuscript.

Line 370: Was LWC measured during this study?

Thanks for the comment. LWC was not measured in the present study. We proposed the possible range of LWC through the comparison of number fraction of scavenged particles with previous studies. As shown in Lines 319-328, relatively lower

scavenging efficiency in the present study was most likely attributed to less dense clouds (with a liquid water content or LWC < 0.1 g m^{-3}). Generally, the half activated diameter increases with decreasing LWC. Henning et al. (2002) stated that particles with d_{ve} = 700 nm were only half activated with LWC < 0.1 g m^{-3}, in contrast, particles with d_{ve} = ~100 nm can be half activated when the LWC > 0.15 g m^{-3}. Similarly, Hammer et al. (2014) showed that only particles with a d_{ve} larger than 300 - 500 nm could be activated under low-LWC conditions (LWC < 0.1 g m^{-3}), which is a typical condition for the formation of fog at the ground level.

Figure captions: Refrain from including discussion and references in the figure captions (keep this in the text body).

Thanks for the comment. We have moved the discussion in Figure 4 to the text, please refer to Lines 284-288 of the revised manuscript.

Figure 1: Report units on the y-axis.

Figure 1 has been revised as suggested.

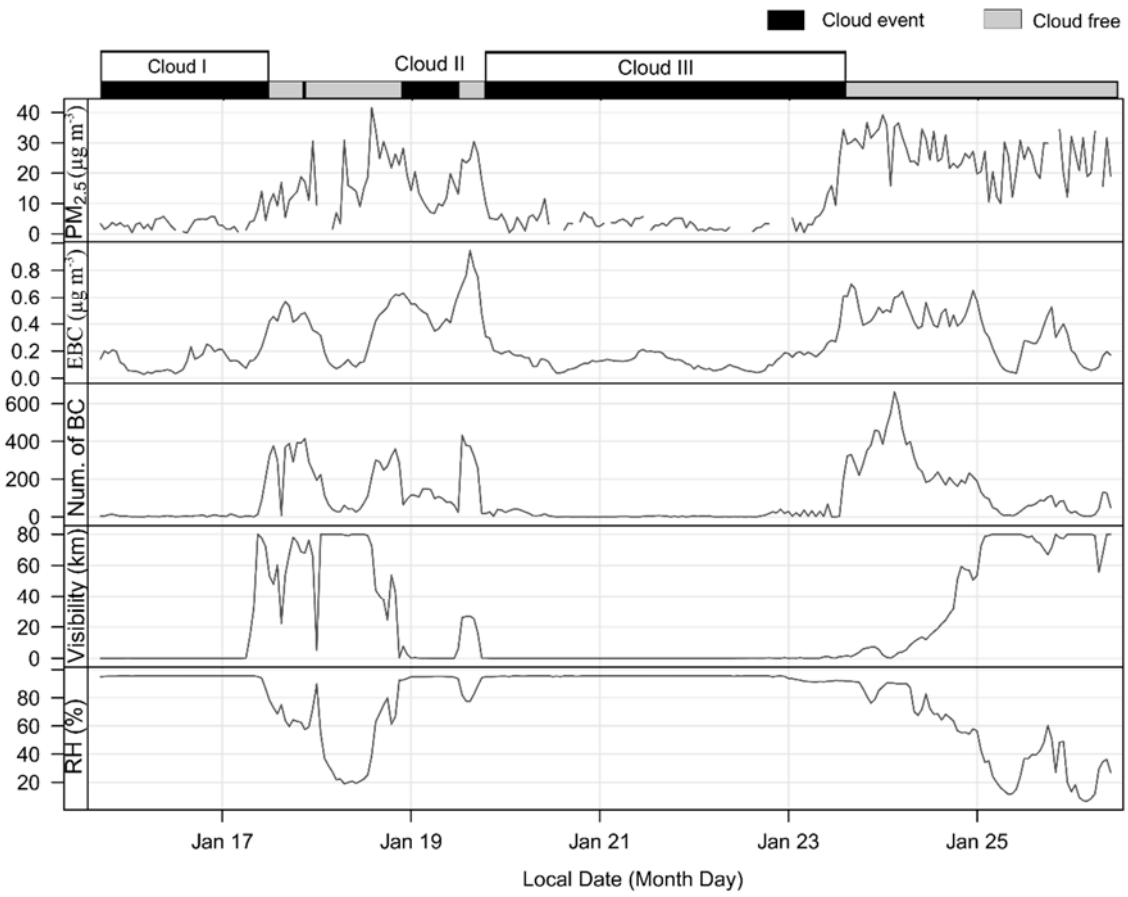

Fig. 1. Temporal profiles (with a 1 hour resolution) of PM2.5, EBC mass concentrations, number of BC-containing particles by SPAMS, RH and visibility. Three cloud events are illustrated with black bars above the figure. $PM_{2.5}$ during the cloud events corresponded to the cloud INT particles. EBC and number of BC-containing particles data were shown for all categories, including the cloud-free, cloud RES, and cloud INT particles. The cloud INT particles were only measured during cloud III.

Figure 4: What were the counts normalized to?

The counts were normalized to the average count over the size range. We have added this information in the caption of the Figure 4.

References

Babu, S. S., Moorthy, K. K., Manchanda, R. K., Sinha, P. R., Satheesh, S. K., Vajja, D. P., … Kumar, V. H. A. (2011). Free tropospheric black carbon aerosol measurements using high altitude balloon: Do BC layers build their own homes up in the atmosphere? Geophysical Research Letters, 38(8). https://doi.org/10.1029/2011GL046654.

Cheng, Y. F., et al. (2006), Mixing state of elemental carbon and non-light-absorbing aerosol components derived from in situ particle optical properties at Xinken in Pearl River Delta of China, J. Geophys. Res., 111, D20204, doi: 10.1029/2005JD006929.

Liu, D., Flynn, M., Gysel, M., Targino, A., Crawford, I., Bower, K., … Coe, H. (2010). Single particle characterization of black carbon aerosols at a tropospheric alpine site in Switzerland. Atmospheric Chemistry and Physics, 10(15), 7389–7407. https://doi.org/10.5194/acp-10-7389-2010

Pósfai, M., Anderson, J. R., Buseck, P. R., & Sievering, H. (1999). Soot and sulfate aerosol particles in the remote marine troposphere. Journal of Geophysical Research: Atmospheres, 104(D17), 21685–21693. https://doi.org/10.1029/1999JD900208

Pusechel, R. F., Blake, D. F., Snetsinger, K. G., Hansen, A. D. A., Verma, S., & Kato, K. (1992). Black carbon (soot) aerosol in the lower stratosphere and upper troposphere. Geophysical Research Letters, 19(16), 1659–1662.

https://doi.org/10.1029/92GL01801

Schwarz, J. P., Samset, B. H., Perring, A. E., Spackman, J. R., Gao, R. S., Stier, P., … Fahey, D. W. (2013). Global-scale seasonally resolved black carbon vertical profiles over the Pacific. Geophysical Research Letters, 40(20), 5542–5547. https://doi.org/10.1002/2013GL057775

Wang, Q., Huang, R.-J., Cao, J., Han, Y., Wang, G., Li, G., Wang, Y., Dai, W., Zhang, R., and Zhou, Y. (2014). Mixing State of Black Carbon Aerosol in a Heavily Polluted Urban Area of China: Implications for Light Absorption Enhancement. Aerosol Sci. Technol., 48(7):689–697. http://doi.org/10.1080/02786826.2014.917758

Reference

Hammer, E., Gysel, M., Roberts, G. C., Elias, T., Hofer, J., Hoyle, C. R., Bukowiecki, N., Dupont, J. C., Burnet, F., Baltensperger, U., and Weingartner, E.: Size-dependent particle activation properties in fog during the ParisFog 2012/13 field campaign, Atmos. Chem. Phys., 14, 10517-10533, doi:10.5194/acp-14-10517-2014, 2014.

Henning, S., Weingartner, E., Schmidt, S., Wendisch, M., Gaggeler, H. W., and Baltensperger, U.: Size-dependent aerosol activation at the high-alpine site Jungfraujoch (3580 m asl), Tellus B, 54, 82-95, 2002.

Matsui, H.: Black carbon simulations using a size- and mixing-state-resolved three-dimensional model: 2. Aging timescale and its impact over East Asia, J. Geophys. Res.-Atmos., 121, 1808-1821, doi:10.1002/2015jd023999, 2016.

Schroder, J. C., Hanna, S. J., Modini, R. L., Corrigan, A. L., Kreidenwies, S. M., Macdonald, A. M., Noone, K. J., Russell, L. M., Leaitch, W. R., and Bertram, A. K.: Size-resolved observations of refractory black carbon particles in cloud droplets at a marine boundary layer site, Atmos. Chem. Phys., 15, 1367-1383, doi:10.5194/acp-15-1367-2015, 2015.

Shingler, T., Dey, S., Sorooshian, A., Brechtel, F. J., Wang, Z., Metcalf, A., Coggon, M., Mulmenstadt, J., Russell, L. M., Jonsson, H. H., and Seinfeld, J. H.: Characterisation and airborne deployment of a new counterflow virtual impactor inlet, Atmos. Meas. Tech., 5, 1259-1269, doi:10.5194/amt-5-1259-2012, 2012.

Zaveri, R. A., Barnard, J. C., Easter, R. C., Riemer, N., and West, M.: Particle-resolved simulation of aerosol size, composition, mixing state, and the associated optical and cloud condensation nuclei activation properties in an evolving urban plume, J. Geophys. Res.-Atmos., 115, 1383-1392, doi:10.1029/2009jd013616, 2010.

Zhang, G., Lin, Q., Peng, L., Yang, Y., Fu, Y., Bi, X., Li, M., Chen, D., Chen, J., Cai, Z., Wang, X., Peng, P., Sheng, G., and Zhou, Z.: Insight into the in-cloud formation of oxalate based on in situ measurement by single particle mass spectrometry, Atmos. Chem. Phys. Discuss., 2017, 1-39, doi:10.5194/acp-2017-763,

2017.

Zuberi, B., Johnson, K. S., Aleks, G. K., Molina, L. T., and Laskin, A.: Hydrophilic properties of aged soot, Geophys. Res. Lett., 32, 67-106, doi:10.1029/2004gl021496, 2005.

The single-particle mixing state and cloud scavenging of black carbon: a case study at a high-altitude mountain site in southern China

Guohua Zhang [1], Qinhao Lin [1, 2], Long Peng [1, 2], Xinhui Bi [1,*], Duohong Chen [3], Mei Li [4, 5], Lei Li [4, 5], Fred J. Brechtel [6], Jianxin Chen [7], Weijun Yan [7], Xinming Wang [1], Ping'an Peng [1], Guoying Sheng [1], Zhen Zhou [4, 5]

[1]State Key Laboratory of Organic Geochemistry and Guangdong Key Laboratory of Environmental Resources Utilization and Protection, Guangzhou Institute of Geochemistry, Chinese Academy of Sciences, Guangzhou 510640, PR China

[2] University of Chinese Academy of Sciences, Beijing 100039, PR China

[3] State Environmental Protection Key Laboratory of Regional Air Quality Monitoring, Guangdong Environmental Monitoring Center, Guangzhou 510308, PR China

[4] Institute of Mass Spectrometer and Atmospheric Environment, Jinan University, Guangzhou 510632, PR China

[5] Guangdong Provincial Engineering Research Center for on-line source apportionment system of air pollution, Guangzhou 510632, PR China

[6] Brechtel Manufacturing Inc., Hayward, 94544, California, USA

[7] Shaoguan Environmental Monitoring Center, Shaoguan 512026, PR China

Correspondence should be addressed to Xinhui Bi (bixh@gig.ac.cn)

Highlights

- In situ investigation on the cloud scavenging of BC in company with the mixing state was first reported in China.
- The number fraction of scavenged BC-containing particles is close to that of all the measured particles.
- BC-containing particles with higher fractions of organics were scavenged relatively less than those with higher fractions of sulfate.

Abstract

In the present study, a ground-based counterflow virtual impactor (GCVI) was used to sample cloud droplet residual (cloud RES) particles, while a parallel $PM_{2.5}$ inlet was used to sample cloud-free or cloud interstitial (cloud INT) particles. The mixing state of black carbon (BC)-containing particles and the mass concentrations of BC in the cloud-free, RES and INT particles were investigated using a single particle aerosol mass spectrometer (SPAMS) and two aethalometers, respectively, at a mountain site (1690 m a.s.l.) in southern China. The measured BC-containing particles were extensively internally mixed with sulfate, and were scavenged into cloud droplets (0.05–0.45) to a similar (or slightly lower) extent as all the measured particles (0.07–0.6) over the measured size range of 0.1–1.6 μm. The results indicate the preferential activation of larger particles and/or that the production of secondary compositions shifts the BC-containing particles towards larger sizes. BC-containing particles with an abundance of both sulfate and organics were scavenged less than those with sulfate but limited organics, implying the importance of the mixing state on the incorporation of BC-containing particles into cloud droplets. The mass scavenging efficiency of BC with an average of 33% was similar for different cloud events independent of the air mass. This is the first time that both the mixing state and cloud scavenging of BC in China have been reported. Our results would improve the knowledge on the concentration, mixing state, and cloud scavenging of BC in the free troposphere.

Keywords: black carbon, cloud droplet residual particles, mixing state, cloud scavenging, interstitial particle

1 Introduction

Black carbon (BC), also known as soot or elemental carbon, is primarily emitted from incomplete combustion processes (Bond et al., 2013; Petzold et al., 2013). Fresh BC-containing particles are generally hydrophilic due to the presence of thin coatings of inorganic or organic materials (Zuberi et al., 2005), and during transport they become more hydrophilic when further coated through coagulation, condensation and photochemical oxidation (Zuberi et al., 2005; Zaveri et al., 2010; Matsui, 2016). Hydrophilic BC-containing particles can act as cloud condensation nuclei (CCN) and thus modify cloud microphysical properties (Straub et al., 2012; Schroder et al., 2015; Roth et al., 2016). The increase in CCN activity enhances the in-cloud scavenging of BC and thus reduces its lifetime (Zaveri et al., 2010). Aerosol-cloud interactions represent one of the largest uncertainties in our current understanding of human-induced climate forcing (McFiggans et al., 2006; Andreae and Rosenfeld, 2008). Therefore, a more comprehensive understanding of how aerosol particles form cloud droplets is required in order to reduce the uncertainty of the impacts of aerosols on the climate (Furutani et al., 2008).

The abilities of particles to act as CCN are largely controlled by their sizes and chemical compositions or mixing state (Dusek et al., 2006; Cubison et al., 2008; Kammermann et al., 2010; Baustian et al., 2012; Ching et al., 2012). Larger aerosol particles were found to be more easily scavenged into cloud droplets (Drewnick et al., 2007). Zhou et al. (2009) found higher scavenging rates for sulfate, nitrate and BC than those for organics at Mount Tai in northern China. At the same site, 92% of the cloud residual particles were attributed to

sulfate-related salts (Li et al., 2011b). On the other hand, the chemical compositions of the original CCN could be altered after the evaporation of the cloud droplets through the effective formation of secondary aerosol compositions during cloud processing (Hayden et al., 2008; Herrmann et al., 2015; Roth et al., 2016). The mixing state of BC-containing particles is of high concern, since their activation as CCN is primarily attributed to the presence of secondary coatings (Lambe et al., 2015; Schroder et al., 2015). Additionally, the mixing state of BC-containing particles is complex and constantly changing in the atmosphere, and they are highly influenced by the particle size, sources, the formation of secondary species and transport processes (Cahill et al., 2012; Healy et al., 2012; Zhang et al., 2014).

Recent in situ studies of cloud droplets have provided the most direct information on the incorporation of BC into clouds. The mass scavenging efficiency was observed to be in a range of 33–74% for BC, which was higher with increasing particle sizes at the Puy de Dome (1465 m a.s.l.), France (Sellegri et al., 2003). It ranged from 13% to 50% corresponding to different air masses at a coastal Chilean hill (450 m a.s.l.) (Heintzenberg et al., 2016). Cozic et al. (2007) reported a scavenging rate of BC similar to those of bulk aerosols due to its internal mixing state with soluble materials. Wang et al. (2012) showed a higher scavenging efficiency for BC than those for organics. Roth et al. (2016) found an enhanced contribution of BC-containing particles in cloud residual particles compared to that in interstitial particles. However, Zelenyuk et al. (2010) observed negligible BC in cloud droplet residual particles above Alaska, USA. Therefore, an in-depth study on the composition, size and mixing state

of BC in cloud droplets and interstitial particles is necessary for a better understanding of the interactions between BC and cloud droplets, and the influences of anthropogenic emissions on cloud formation in the free troposphere.

Single-particle mass spectrometry (SPMS) studies on fog interstitial particles and droplet residual particles were performed previously at an urban site in southern China (Zhang et al., 2012; Bi et al., 2016). The predominance of BC-containing particles serving as effective fog condensation nuclei highlights the important influence of anthropogenic emissions on the public environment and regional climate (Bi et al., 2016). However, there are no direct observations of the cloud scavenging of BC or the mixing states of cloud interstitial (cloud INT) and droplet residual (cloud RES) BC-containing particles in the high-altitude atmosphere or the free troposphere above China to date. Therefore, the size-resolved mixing state and the scavenging efficiency of BC-containing particles were investigated at a high-altitude site to further our knowledge of (1) the mixing state of BC-containing particles, (2) the influence of the mixing state on the incorporation of BC into cloud droplets, and (3) the influence of anthropogenic activities on cloud formation in the free troposphere above southern China.

2 Methods

2.1 Sampling setup

The observations of cloud events were conducted at the National Atmospheric Background Monitoring Station in Nanling of Guangdong Province, which is located on the

top of Mount Tianjing (24°41′56″N, 112°53′56″E, 1690 m a.s.l.) in southern China, from 16 to 26 Jan 2016. The average boundary layer height (https://www.arl.noaa.gov) at the site over the study is ~280 m compared to the surrounding ground altitude (~500 m) for this region. It is reasonable to consider this site sampling free tropospheric air throughout the study. The site is located in a natural preserve distant from anthropogenic activities. A map of the location and terrain of the site can be found elsewhere (Lin et al., 2017).

Aerosols were introduced into the instruments through two parallel sampling lines. The first inlet is a ground-based counterflow virtual impactor (GCVI) (Model 1205, Brechtel Mfg., Inc., USA) (Bi et al., 2016). The GCVI employs a compact wind tunnel upstream of the CVI inlet (Model 1204) to accelerate fog and cloud droplets into the CVI inlet tip. Similar methodologies have been extensively applied to collect fog/cloud RES particles (e.g., Sorooshian et al., 2013; Roth et al., 2016; van Pinxteren et al., 2016). The detail information on the design of the CVI inlet and testing on the size-resolved transmission efficiency of droplets can be found elsewhere (Shingler et al., 2012). The inlet cut size was set to be 8 μm, at which the transmission efficiency of droplets is 50%. The enhancement factor (EF) was calculated according to the equation (Shingler et al., 2012): $EF = A_{tip}*V_{air}/q_{sample}$, where A_{tip} is the area of the inlet tip where drops enter, V_{air} is wind tunnel velocity, and q_{sample} is the volumetric flow rate of sampled air in the CVI inlet. A_{tip} is 1.67×10^{-5} m^2, q_{sample} is 15 l min^{-1}, and V_{air} was set to be ~80 m/s, coincides with an EF of 5.25. Therefore, the reported mass concentrations for the cloud RES particles in the following text were first divided by 5.25. The sampled cloud droplets enter the evaporation chamber (with an airflow temperature of

40 °C), where the droplets are dried, thereby leaving behind cloud RES particles that were CCN. The influence of background particles on the collection of the cloud RES particles could be negligible. A test on the cloud-free air showed that the average particles number concentration sampled by the GCVI was ~1 cm^{-3}, far below the level (~2000 cm^{-3}) air over the study (Zhang et al., 2017). A testing before measurements demonstrates that the influence of background aerosols on the collection of cloud droplets could be negligible (Zhang et al., 2017). The ambient inlet is a $PM_{2.5}$ sampling line that delivers ambient particles during cloud-free periods or cloud INT particles during cloud events. Cloud INT particles were regarded as $PM_{2.5}$ during the cloud events. More detailed description on the sampling can be found in the companion papers (Lin et al., 2017; Zhang et al., 2017).

Cloud events were characterized by a sudden drop in visibility and a sharp increase in the relative humidity (RH) measured by the GCVI. An upper-limit visibility threshold of 5 km and a lower-limit RH threshold of 95% were established to identify the cloud events and trigger the sampling of the cloud RES particles.

An illustrative scheme of the instrumentation setup is provided in Fig. S1 in the Supporting Information (SI). Downstream of the GCVI, an aethalometer (Model AE-33, Magee Scientific, USA), a single particle aerosol mass spectrometer (SPAMS, Hexin Analytical Instrument Co., Ltd.) and a scanning mobility particle sizer (SMPS, MSP Corporation, USA) were used to measure the concentration of BC, the size-resolved mixing state of the collected particles, and the number size distribution of submicron particles, respectively. Downstream of the ambient inlet, an SMPS (Grimm 5.041, Germany), an

aethalometer (Model AE-31, Magee Scientific, USA), and a tapered element oscillating microbalance (Model 1405, Thermo Scientific, USA) were used to determine the number size distribution of submicron particles and the mass concentrations of BC and $PM_{2.5}$, respectively. During the cloud-free periods, the instruments downstream of the GCVI were manually shifted and connected to the ambient $PM_{2.5}$ inlet. During the present study, three cloud events (Cloud I, II, III, each with a RH constantly above 95% for more than 12 hours) were encountered and identified by the GCVI (Lin et al., 2017), as shown in Fig. 1. During Cloud I and II, the cloud RES particles provided by the GCVI were measured by the instruments downstream of the GCVI. During Cloud III, the cloud RES and cloud INT particles were intermittently measured by these instruments at approximately one-hour intervals.

2.2 Determinations of the mass concentrations of BC

The AE–31 and AE–33 measured the BC concentration at the wavelength of 880 nm, which is typically represented as equivalent BC (EBC) (Petzold et al., 2013). The EBC concentration reported in the present study was measured using the AE–33 described in a great detail elsewhere (Drinovec et al., 2015). The limitations and uncertainties of the AE-31 in measuring BC and the necessary corrections were well documented (Weingartner et al., 2003; Arnott et al., 2005; Backman et al., 2016). A brief description of this issue is provided in the Supplement.

178 **2.3 Identification of BC-containing particles by the SPAMS**

179 Both the vacuum aerodynamic diameter (d_{va}) and the chemical compositions of the
180 individual particles were analyzed by the SPAMS, as briefly described in the Supplement. A
181 detailed description of the performance and the calibrations of the SPAMS can be found
182 elsewhere (Li et al., 2011a). The mass spectra for ~75000 particles with d_{va} values in the
183 range of 0.1-1.6 μm were obtained by the SPAMS over the study. The diameter is
184 represented herein as d_{va} rather than the equivalent volume diameter (d_{ve}), the conversion
185 for which can be found in the supplement (DeCarlo et al., 2004; Hu et al., 2012). An
186 adaptive resonance theory-based neural network algorithm (ART-2a) was applied to cluster
187 the individual particles based on the presence and intensities of ion peaks (Song et al., 1999)
188 with a vigilance factor of 0.7, a learning rate of 0.05, and 20 iterations. Three BC particle
189 types were obtained: the mass spectra of particles with more carbon cluster ions ($C_n^{+/-}$, $n > 6$)
190 and sulfate (BC-sul1), those with fewer carbon cluster ions ($C_n^{+/-}$, $n \leq 6$) and more intense
191 sulfate (BC-sul2), and those with an abundance of both sulfate and organics (BC-OC-sul).
192 The relative amount of OC to BC for the BC-OC-sul particles is significantly larger than
193 that in the BC-sul1 and BC-sul2 particles, as indicated in Fig. S2. Over all of the detected
194 BC-containing particles, the BC-sul2 type is the most abundant (63%) particle type,
195 followed by the BC-sul1 (21%) and BC-OC-sul (16%) types. More detailed information
196 regarding the other particle types can be found elsewhere (Lin et al., 2017).
197

198 **3 Results and Discussion**

During the sampling periods, the temperature and RH generally varied between –9.9 - 11.4 °C and 6.7 - 100%, respectively. The sampling durations for the cloud-free, cloud RES and cloud INT (only detected in Cloud III) particles were approximately 109, 123, and 26 hours, respectively. The detected numbers of the cloud-free, cloud RES, and cloud INT particles by the SPAMS were 48835, 23616, and 1063, respectively. The average number fractions of BC-containing particles in the cloud-free, cloud RES, and cloud INT particles were 44%, 49%, and 53%, respectively. The number fractions of BC-containing particles that were incorporated within the cloud droplets ranged between those observed at an urban site (70%) in southern China (Bi et al., 2016) and those observed at a mountain site (~30%) in Germany (Roth et al., 2016). While some mineral dust might trigger heterogeneous ice nucleation at temperatures below –7 °C (Atkinson et al., 2013), this would not influence the discussion on the number fraction and chemistry of the cloud RES BC-containing particles. The cloud RES BC-containing particles only accounted for ~0.1% of all the detected ones in a 2-hour window when the average temperature was ~ –7 °C.

Air masses from the southwestern continental and marine areas dominated throughout the sampling period, carrying relatively warmer and wetter air masses that benefited the formation of clouds based on the back-trajectory analysis (Lin et al., 2017). Cloud II was strongly influenced by a northeastern air mass in contrast to the southwestern air mass that dominated during Cloud I and III. As shown in Fig. 2, the air mass during Cloud II represents relatively polluted conditions. The mass concentration of EBC during Cloud II was approximately 200 ng m^{-3}, which is four times that (~50 ng m^{-3}) observed during the

other two events. Similarly, the number fraction of the BC-containing particles in the cloud RES particles during Cloud II (~60%) was higher than those during the other two cloud events (< 30%). This case might provide partial evidence for the influence of anthropogenic emissions and atmospheric transport on the formation of clouds at the remote high-altitude site in southern China.

3.1 Mixing state of BC for cloud-free, residual, and interstitial particles

The dominant ion peaks for the cloud-free, cloud RES, and cloud INT BC-containing particles were those of carbon cluster ions ($C_n^{+/-}$, n = 1, 2, 3, …), OC fragments (m/z 27$[C_2H_3]^+$, -26$[CN]^-$, 37$[C_3H]^+$, and 43$[C_2H_3O]^+$), and secondary inorganic species, such as sulfate (-97$[HSO_4]^-$), nitrate (-62$[NO_3]^-$ and -46$[NO_2]^-$), and ammonium (18$[NH_4]^+$) (Zhang et al., 2014). The cloud-free BC-containing particles were internally mixed to a great extent with detectable sulfate (97% by number), nitrate (50%), oxidized organics (43$[C_2H_3O]^+$, 72%), and/or ammonium (79%), as presented in Fig. S3. A similar mixing state of the BC-containing particles has been observed at both urban and mountain sites (Moffet and Prather, 2009; Li et al., 2011c; Cahill et al., 2012). The overwhelming association of BC with sulfate strongly indicates a substantial influence of anthropogenic emissions of sulfate precursors (e.g., SO_2) on the aging of BC (Huang and Yu, 2008; Khalizov et al., 2009; Guo et al., 2012; Peng et al., 2016), which directly enhances the incorporation of BC into clouds as discussed in section 3.2. Compared to the BC-containing particles at urban and suburban sites that are situated close to emission sources, the relative amounts of sulfate and

ammonium substantially increased for those at the mountain site, as shown in Fig. S4. The relative peak area (RPA) of each m/z relative to the sum of the peak areas in a mass spectrum was applied herein to represent the relative amount of a species in a particle (e.g., Jeong et al., 2011; Xing et al., 2011; Healy et al., 2013). The enhancement of sulfate in the atmosphere above southern China is reasonable since sulfate accounts for the largest portion of the compositions in this region and should be mainly associated with ammonium (Zhang et al., 2013). As expected, the temporal variations of the RPAs were significantly correlated ($p < 0.01$) between ammonium and sulfate (Fig. S5). These species were generally regarded as secondary components, and thus, such high fractions of the internal mixing state and the enhancement of ammonium and sulfate at the high-altitude site demonstrates a highly aged state of the BC-containing particles.

As shown in Fig. 3, the secondary components were enhanced in the cloud RES BC-containing particles relative to the cloud INT BC-containing particles. The enhancement was more obvious for sulfate rather than for ammonium, oxidized organics or nitrate. The enhancement of sulfate in cloud RES particles has been broadly observed (Kamphus et al., 2010; Zelenyuk et al., 2010; Hiranuma et al., 2011). A comparison of the size distributions of the cloud RES and cloud INT BC-containing particles (Fig. 4) further suggests that the in-cloud addition of secondary components shifted the BC-containing particles towards larger sizes, which is discussed in the following section. Overall, our observations suggest that the BC-containing particles were heavily coated at the high-altitude site before they were incorporated into the cloud droplets and that the

in-cloud production of coating materials (e.g., ammonium sulfate) was present. Although an abundance of BC-coated materials was also observed at Mt. Soledad by a single particle soot photometer (Schroder et al., 2015), the chemical compositions of the coated materials cannot be obtained to provide further information on the mixing state of BC. Our analysis further reflects the importance of the chemical mixing state on the cloud processing of BC.

The role of the mixing state on the scavenging of the BC-containing particles was further investigated through a comparison of the individual particle types of the cloud-free, cloud RES, and cloud INT BC-containing particles. As shown in Fig. 5, the number fraction of BC-OC-sul (~8%) was much lower in the cloud RES than those (~25%) in the cloud-free and cloud INT BC-containing particles. Despite the different distributions of the BC particle types, the BC-sul1 and BC-sul2 types were dominant, while the BC-OC-sul type contributed only a limited fraction to the cloud RES BC-containing particles during each of the cloud events. Consistently, the Nf_{act} of the BC-OC-sul particles was generally lower than 0.1 over the detected size range, which is much lower than those for the BC-sul1 and BC-sul2 types (Fig. S6). Distinct differences in the mixing state accompanied the observations of cloud RES BC-containing particles. The cloud RES BC-containing particles with more sulfate and fewer organics were observed more frequently than those with more organics and less sulfate (Fig. 5).

3.2 Fractions of BC incorporated into cloud droplets

3.2.1 Size-resolved scavenging of BC-containing particles

The normalized number size distributions of the cloud-free, cloud RES, and cloud INT BC-containing particles are shown in Fig. 4. A representative comparison between the size distributions measured by the SPAMS and the SMPS can be found in Fig. S7. While these distributions do not represent the actual particle number size distributions due to the decreasing detection efficiencies at smaller sizes (Allen et al., 2000; Wenzel et al., 2003; Qin et al., 2006), they could reflect the importance of the particle size on the incorporation of BC-containing particles into cloud droplets (Dusek et al., 2006; Matsui, 2016). The cloud RES BC-containing particles had the largest size mode, followed by the cloud-free BC-containing particles, with the cloud INT BC-containing particles in the smallest size mode. These size distribution patterns are indicative of the preferential activation of larger particles and/or the addition of secondary species during in-cloud processing, and are consistent with those of previous studies (Drewnick et al., 2007; Zelenyuk et al., 2010; Roth et al., 2016). As expected, the BC-containing particles were internally mixed with increasingly higher intensities of sulfate, ammonium and oxidized organics with increasing size (Fig. S8). These results are consistent with the observations by Healy et al. (2012) and Zhang et al. (2014) insomuch that larger BC-containing particles were more thickly coated. The BC-containing particles detected by the SPAMS could track the variations of the BC mass concentration in the present study based on a correlation analysis of the time series of the unscaled number of BC-containing particles and the concentration of EBC (Fig. S9). A detailed discussion on the comparison of these two measurements can be found in the Supplement (Yu et al., 2010; Huang et al., 2011; Huang et al., 2012).

The size-resolved scavenged/activated fractions (Nf_{scav}) of the BC-containing particles and all the detected particles were further investigated as a function of their size (Fig. 6). The number fractions of the BC-containing particles incorporated into cloud droplets varied between 0.05–0.45. The Nf_{scav} generally increased with an increase in the size, and those of the BC-containing particles were scavenged to a similar (or slightly lower) extent as those (0.07–0.6) of all the detected particles. The size dependent scavenging of the BC-containing particles is consistent with a modeling study by Matsui (2016). This indicates that the coating materials on the BC-containing particles enhanced their ability to act as CCN (Khalizov et al., 2009; Henning et al., 2012; Roth et al., 2016), consistent with the enhanced internal mixing with secondary soluble species with an increase in the size (Fig. S8) discussed above. The increase of Nf_{scav} with the particle size also suggests that nucleation scavenging is the dominant mechanism for the incorporation of BC-containing particles into cloud droplets (Schroder et al., 2015). These fractions represent a rough estimate because the BC-containing particles in the cloud RES and cloud INT particles were measured intermittently rather than simultaneously.

Relatively lower scavenging efficiency (0.05–0.45) in the present study was most likely attributed to less dense clouds (with a liquid water content or LWC < 0.1 g m^{-3}). Similarly, Matsui (2016) suggested it is not correct to assume all BC-containing particles to be CCN-active in a cloud that has low maximum supersaturation (i.e., 0.1%). Generally, the half activated diameter increases with decreasing LWC. Henning et al. (2002) stated that particles with d_{ve} = 700 nm were only half activated with LWC < 0.1 g m^{-3}, in contrast,

particles with d_{ve} = ~100 nm can be half activated when the LWC > 0.15 g m^{-3}. Similarly, Hammer et al. (2014) showed that only particles with a d_{ve} larger than 300 - 500 nm could be activated under low-LWC conditions (LWC < 0.1 g m^{-3}), which is a typical condition for the formation of fog at the ground level. With an LWC of approximately 0.1 g m^{-3}, Schroder et al. (2015) reported even lower scavenged fractions (0.01–0.1) of BC-containing particles at Mt. Soledad closer to the source region in California, USA. From this perspective, the relatively higher scavenged fractions of the BC-containing particles in the present study compared to those at Mt. Soledad (Schroder et al., 2015) could be mainly attributed to the long-range transport that resulted in the highly aged BC and possibly the higher LWC.

3.2.2 Mass scavenging efficiency of EBC

The concentration of EBC (5^{th} - 95^{th}) obtained using the AE33 for cloud-free air varied over a wide range of 57 - 812 ng m^{-3} with a mean value of 418 ± 248 ng m^{-3}, which accounted for ~2% of the $PM_{2.5}$ on average. The average concentrations of cloud RES and INT EBC were 84 ± 75, and 198 ± 125 ng m^{-3}, respectively. A relatively lower contribution of EBC to the aerosol population supports a substantial addition of secondary aerosols during transport to the high-altitude site, given that EBC represents far more than ~2% of the fine particles near the source regions of southern China (Lan et al., 2013; Wu et al., 2013; Zhang et al., 2013). The observed relatively lower fraction of EBC is consistent with the highly aged state of BC-containing particles at the high-altitude site rather than at urban

and suburban sites, as discussed in section 3.1. The mean concentration is much lower than those observed for urban (6000 ng m^{-3}) and rural (2600 ng m^{-3}) areas (Huang et al., 2012) in southern China. It is similar to those observed at an oceanic site (540 ng m^{-3}) in southern China (Wu et al., 2013) and at the high-altitude Mt. Rax site (430-720 ng m^{-3}) (Hitzenberger et al., 2001). It is several times higher than those at a marine boundary layer site (70 ng m^{-3}) in California, USA (Schroder et al., 2015), the mid-altitude regions (~60 ng m^{-3}) of Nova Scotia, Canada (Chýlek et al., 1996), and the high alpine Jungfraujoch station (50-60 ng m^{-3}) in Switzerland (Cozic et al., 2007). Additional detailed information on the sampling sites and BC concentrations can be found in Table S1. These comparisons suggest that anthropogenic activities have a relatively large impact on the concentration of EBC at the high-altitude site.

It can be seen in Fig. 1 that cloud scavenging could have a strong effect on the decreased particle concentrations (i.e., of EBC and $PM_{2.5}$). A sharp reduction in the particle concentrations were observed at the beginning of the cloud events. The mass-scavenging efficiency of BC ($Mf_{scav,EBC}$), defined as the fraction of EBC incorporated into cloud droplets relative to the total amount of EBC (Cozic et al., 2007), was evaluated as

$$Mf_{scav,EBC} = EBC_{RES}/(EBC_{RES} + EBC_{INT}) \times 100\% \quad (R1)$$

Since the EBC_{RES} and EBC_{INT} were not simultaneously obtained using the AE-33, the EBC_{INT} measured concurrently by the AE-31 was applied in the calculation. The EBC measured using the AE-31 is significantly correlated ($R^2 = 0.9$, $p < 0.001$) with and only slightly lower than that measured by the AE-33, as shown in Fig. S10. This validates the

calculation in R1. The overall uncertainty in the $Mf_{scav,EBC}$ is within 10%, as assessed in the supplement. The measurements of EBC and the sampling of the cloud RES particles were regarded as the main influential factors.

The $Mf_{scav,EBC}$ ranged between 15 - 54% (5^{th} - 95^{th}) with an average value of approximately 33%. The $Mf_{scav,EBC}$ in this study is within the range of those values (33-54%) reported for mid-altitude (approximately 1500 m) mountain sites, generally lower than those reported (45-74%) for high-altitude (approximately 3000 m) mountain sites, and higher than those reported (6-15%) for ground sites (Cozic et al., 2007 and references therein). The differences among the various observations are generally attributed to the water content and the sizes and mixing state of the BC-containing particles (Cozic et al., 2007). The $Mf_{scav,EBC}$ was not so different for the cloud events (Fig. S11) impacted by different air masses, which is consistent with the highly aged state of the BC observed in this study. These results indicate that the incorporation of BC into clouds was dominantly controlled by its mixing state rather than other factors (e.g., the air mass or the concentration of EBC) under low-LWC conditions (e.g., < 0.1 g m^{-3}).

4 Conclusions

The influences of the size and mixing state on the incorporation of BC in clouds were investigated at a remote high-altitude mountain site in southern China. On average, the mass concentration of EBC was 418 ± 248, 84 ± 75, and 198 ± 125 ng m^{-3} for the cloud-free, cloud RES, and cloud INT particles, respectively. The BC was highly aged through the

predominant accumulation of sulfate during transport. BC-containing particles were found to be scavenged in the cloud phase to a similar extent as bulk aerosols. The size-resolved scavenged fraction of BC-containing particles was estimated to be in a range of 0.05–0.45; it increased with an increase in the size and was mainly controlled by the mixing state with secondary soluble species. This data is restricted to particles in the size range of 0.1-1.6 μm, and thus, particles with sizes smaller than 0.1 μm that might serve as CCN are beyond the scope of this study. The mass-scavenging efficiency of BC varied between 15–54% and was independent of the air mass. This paper provides the first direct evidence on the substantial contribution of BC-containing particles to cloud droplet residual particles in the free troposphere of southern China. Our results also suggest that it might be appropriate to consider BC-containing particles as a highly aged state in the free troposphere in future studies. The data are also useful for constraining models used for predicting BC concentrations in the free troposphere.

Acknowledgement

This work was supported by the National Key Research and Development Program of China (2017YFC0210104), the National Natural Science Foundation of China (No. 91544101 and 41775124), the Foundation for Leading Talents of the Guangdong Province Government, and the State Key Laboratory of Organic Geochemistry (SKLOGA201603A and SKLOGC201604).

References

Allen, J. O., Fergenson, D. P., Gard, E. E., Hughes, L. S., Morrical, B. D., Kleeman, M. J., Gross, D. S., Galli, M. E., Prather, K. A., and Cass, G. R.: Particle detection efficiencies of aerosol time of flight mass spectrometers under ambient sampling conditions, Environ. Sci. Technol., 34, 211-217, 2000.

Andreae, M. O., and Rosenfeld, D.: Aerosol–cloud–precipitation interactions. Part 1. The nature and sources of cloud-active aerosols, Earth-Sci. Rev., 89, 13-41, doi:http://dx.doi.org/10.1016/j.earscirev.2008.03.001, 2008.

Arnott, W. P., Hamasha, K., Moosmuller, H., Sheridan, P. J., and Ogren, J. A.: Towards aerosol light-absorption measurements with a 7-wavelength Aethalometer: Evaluation with a photoacoustic instrument and 3-wavelength nephelometer, Aerosol Sci. Tech., 39, 17-29, doi:10.1080/027868290901972, 2005.

Atkinson, J. D., Murray, B. J., Woodhouse, M. T., Whale, T. F., Baustian, K. J., Carslaw, K. S., Dobbie, S., O'Sullivan, D., and Malkin, T. L.: The importance of feldspar for ice nucleation by mineral dust in mixed-phase clouds, Nature, 498, 355-358, doi:10.1038/nature12278, 2013.

Backman, J., Schmeisser, L., Virkkula, A., Ogren, J. A., Asmi, E., Starkweather, S., Sharma, S., Eleftheriadis, K., Uttal, T., Jefferson, A., Bergin, M., and Makshtas, A.: On Aethalometer measurement uncertainties and multiple scattering enhancement in the Arctic, Atmos. Meas. Tech. Discuss., 2016, 1-31, doi:10.5194/amt-2016-294, 2016.

Baustian, K. J., Cziczo, D. J., Wise, M. E., Pratt, K. A., Kulkarni, G., Hallar, A. G., and Tolbert, M. A.: Importance of aerosol composition, mixing state, and morphology for heterogeneous ice nucleation: A combined field and laboratory approach, J. Geophys. Res., 117, 2240-2260, doi:10.1029/2011jd016784, 2012.

Bi, X. H., Lin, Q. H., Peng, L., Zhang, G. H., Wang, X. M., Brechtel, F. J., Chen, D. H., Li, M., Peng, P. A., Sheng, G. Y., and Zhou, Z.: In situ detection of the chemistry of individual fog droplet residues in the Pearl River Delta region, China, J. Geophys. Res.-Atmos., 121, 9105-9116, doi:10.1002/2016JD024886, 2016.

436 Bond, T. C., Doherty, S. J., Fahey, D. W., Forster, P. M., Berntsen, T., DeAngelo, B. J.,
437 Flanner, M. G., Ghan, S., Karcher, B., Koch, D., Kinne, S., Kondo, Y., Quinn, P. K., Sarofim,
438 M. C., Schultz, M. G., Schulz, M., Venkataraman, C., Zhang, H., Zhang, S., Bellouin, N.,
439 Guttikunda, S. K., Hopke, P. K., Jacobson, M. Z., Kaiser, J. W., Klimont, Z., Lohmann, U.,
440 Schwarz, J. P., Shindell, D., Storelvmo, T., Warren, S. G., and Zender, C. S.: Bounding the role
441 of black carbon in the climate system: A scientific assessment, J. Geophys. Res.-Atmos., 118,
442 5380-5552, doi:10.1002/Jgrd.50171, 2013.
443 Cahill, J. F., Suski, K., Seinfeld, J. H., Zaveri, R. A., and Prather, K. A.: The mixing state
444 of carbonaceous aerosol particles in northern and southern California measured during CARES
445 and CalNex 2010, Atmos. Chem. Phys., 12, 10989-11002, doi:10.5194/acp-12-10989-2012,
446 2012.
447 Chýlek, P., Banic, C. M., Johnson, B., Damiano, P. A., Isaac, G. A., Leaitch, W. R., Liu, P.
448 S. K., Boudala, F. S., Winter, B., and Ngo, D.: Black carbon: Atmospheric concentrations and
449 cloud water content measurements over southern Nova Scotia, J. Geophys. Res.-Atmos., 101,
450 29105-29110, doi:10.1029/95JD03433, 1996.
451 Ching, J., Riemer, N., and West, M.: Impacts of black carbon mixing state on black carbon
452 nucleation scavenging: Insights from a particle-resolved model, J. Geophys. Res.-Atmos., 117,
453 1-21, 2012.
454 Cozic, J., Verheggen, B., Mertes, S., Connolly, P., Bower, K., Petzold, A., Baltensperger,
455 U., and Weingartner, E.: Scavenging of black carbon in mixed phase clouds at the high alpine
456 site Jungfraujoch, Atmos. Chem. Phys., 7, 1797-1807, 2007.
457 Cubison, M. J., Ervens, B., Feingold, G., Docherty, K. S., Ulbrich, I. M., Shields, L.,
458 Prather, K., Hering, S., and Jimenez, J. L.: The influence of chemical composition and mixing
459 state of Los Angeles urban aerosol on CCN number and cloud properties, Atmos. Chem. Phys.,
460 8, 5649-5667, 2008.
461 DeCarlo, P. F., Slowik, J. G., Worsnop, D. R., Davidovits, P., and Jimenez, J. L.: Particle
462 morphology and density characterization by combined mobility and aerodynamic diameter

463 measurements. Part 1: Theory, Aerosol Sci. Tech., 38, 1185-1205,
464 doi:10.1080/027868290903907, 2004.
465 Drewnick, F., Schneider, J., Hings, S. S., Hock, N., Noone, K., Targino, A., Weimer, S.,
466 and Borrmann, S.: Measurement of ambient, interstitial, and residual aerosol particles on a
467 mountaintop site in central Sweden using an aerosol mass spectrometer and a CVI, J. Atmos.
468 Chem., 56, 1-20, doi:10.1007/s10874-006-9036-8, 2007.
469 Drinovec, L., Močnik, G., Zotter, P., Prévôt, A. S. H., Ruckstuhl, C., Coz, E., Rupakheti,
470 M., Sciare, J., Müller, T., Wiedensohler, A., and Hansen, A. D. A.: The "dual-spot"
471 Aethalometer: an improved measurement of aerosol black carbon with real-time loading
472 compensation, Atmos. Meas. Tech., 8, 1965-1979, doi:10.5194/amt-8-1965-2015, 2015.
473 Dusek, U., Frank, G. P., Hildebrandt, L., Curtius, J., Schneider, J., Walter, S., Chand, D.,
474 Drewnick, F., Hings, S., Jung, D., Borrmann, S., and Andreae, M. O.: Size matters more than
475 chemistry for cloud-nucleating ability of aerosol particles, Science, 312, 1375-1378,
476 doi:10.1126/science.1125261, 2006.
477 Furutani, H., Dall'osto, M., Roberts, G. C., and Prather, K. A.: Assessment of the relative
478 importance of atmospheric aging on CCN activity derived from field observations, Atmos.
479 Environ., 42, 3130-3142, doi:10.1016/j.atmosenv.2007.09.024, 2008.
480 Guo, J., Wang, Y., Shen, X. H., Wang, Z., Lee, T., Wang, X. F., Li, P. H., Sun, M. H.,
481 Collett, J. L., Wang, W. X., and Wang, T.: Characterization of cloud water chemistry at Mount
482 Tai, China: Seasonal variation, anthropogenic impact, and cloud processing, Atmos. Environ.,
483 60, 467-476, doi:10.1016/j.atmosenv.2012.07.016, 2012.
484 Hammer, E., Gysel, M., Roberts, G. C., Elias, T., Hofer, J., Hoyle, C. R., Bukowiecki, N.,
485 Dupont, J. C., Burnet, F., Baltensperger, U., and Weingartner, E.: Size-dependent particle
486 activation properties in fog during the ParisFog 2012/13 field campaign, Atmos. Chem. Phys.,
487 14, 10517-10533, doi:10.5194/acp-14-10517-2014, 2014.
488 Hayden, K. L., Macdonald, A. M., Gong, W., Toom-Sauntry, D., Anlauf, K. G., Leithead,
489 A., Li, S. M., Leaitch, W. R., and Noone, K.: Cloud processing of nitrate, J. Geophys.
490 Res.-Atmos., 113, 1-18, doi:10.1029/2007jd009732, 2008.

491 Healy, R. M., Sciare, J., Poulain, L., Kamili, K., Merkel, M., Muller, T., Wiedensohler, A.,
492 Eckhardt, S., Stohl, A., Sarda-Esteve, R., McGillicuddy, E., O'Connor, I. P., Sodeau, J. R., and
493 Wenger, J. C.: Sources and mixing state of size-resolved elemental carbon particles in a
494 European megacity: Paris, Atmos. Chem. Phys., 12, 1681-1700,
495 doi:10.5194/acp-12-1681-2012, 2012.
496 Healy, R. M., Sciare, J., Poulain, L., Crippa, M., Wiedensohler, A., Prevot, A. S. H.,
497 Baltensperger, U., Sarda-Esteve, R., McGuire, M. L., Jeong, C. H., McGillicuddy, E.,
498 O'Connor, I. P., Sodeau, J. R., Evans, G. J., and Wenger, J. C.: Quantitative determination of
499 carbonaceous particle mixing state in Paris using single-particle mass spectrometer and aerosol
500 mass spectrometer measurements, Atmos. Chem. Phys., 13, 9479-9496,
501 doi:10.5194/acp-13-9479-2013, 2013.
502 Heintzenberg, J., Cereceda-Balic, F., Vidal, V., and Leck, C.: Scavenging of black carbon
503 in Chilean coastal fogs, Sci. Total. Environ., 541, 341-347, 2016.
504 Henning, S., Weingartner, E., Schmidt, S., Wendisch, M., Gaggeler, H. W., and
505 Baltensperger, U.: Size-dependent aerosol activation at the high-alpine site Jungfraujoch (3580
506 m asl), Tellus B, 54, 82-95, 2002.
507 Henning, S., Ziese, M., Kiselev, A., Saathoff, H., Mohler, O., Mentel, T. F., Buchholz, A.,
508 Spindler, C., Michaud, V., Monier, M., Sellegri, K., and Stratmann, F.: Hygroscopic growth
509 and droplet activation of soot particles: uncoated, succinic or sulfuric acid coated, Atmos.
510 Chem. Phys., 12, 4525-4537, doi:10.5194/acp-12-4525-2012, 2012.
511 Herrmann, H., Schaefer, T., Tilgner, A., Styler, S. A., Weller, C., Teich, M., and Otto, T.:
512 Tropospheric Aqueous-Phase Chemistry: Kinetics, Mechanisms, and Its Coupling to a
513 Changing Gas Phase, Chem. Rev., 115, 4259-4334, doi:10.1021/cr500447k, 2015.
514 Hiranuma, N., Kohn, M., Pekour, M. S., Nelson, D. A., Shilling, J. E., and Cziczo, D. J.:
515 Droplet activation, separation, and compositional analysis: laboratory studies and atmospheric
516 measurements, Atmos. Meas. Tech., 4, 2333-2343, doi:10.5194/amt-4-2333-2011, 2011.

517 Hitzenberger, R., Berner, A., Glebl, H., Drobesch, K., Kasper-Giebl, A., Loeflund, M.,
518 Urban, H., and Puxbaum, H.: Black carbon (BC) in alpine aerosols and cloud water -
519 concentrations and scavenging efficiencies, Atmos. Environ., 35, 5135-5141, 2001.
520 Hu, M., Peng, J. F., Sun, K., Yue, D. L., Guo, S., Wiedensohler, A., and Wu, Z. J.:
521 Estimation of Size-Resolved Ambient Particle Density Based on the Measurement of Aerosol
522 Number, Mass, and Chemical Size Distributions in the Winter in Beijing, Environ. Sci.
523 Technol., 46, 9941-9947, doi:10.1021/Es204073t, 2012.
524 Huang, X. F., and Yu, J. Z.: Size distributions of elemental carbon in the atmosphere of a
525 coastal urban area in South China: characteristics, evolution processes, and implications for the
526 mixing state, Atmos. Chem. Phys., 8, 5843-5853, 2008.
527 Huang, X. F., Gao, R. S., Schwarz, J. P., He, L. Y., Fahey, D. W., Watts, L. A.,
528 McComiskey, A., Cooper, O. R., Sun, T. L., Zeng, L. W., Hu, M., and Zhang, Y. H.: Black
529 carbon measurements in the Pearl River Delta region of China, J. Geophys. Res., 116, 445-451,
530 doi:10.1029/2010jd014933, 2011.
531 Huang, X. F., Sun, T. L., Zeng, L. W., Yu, G. H., and Luan, S. J.: Black carbon aerosol
532 characterization in a coastal city in South China using a single particle soot photometer, Atmos.
533 Environ., 51, 21-28, doi:10.1016/j.atmosenv.2012.01.056, 2012.
534 Jeong, C. H., McGuire, M. L., Godri, K. J., Slowik, J. G., Rehbein, P. J. G., and Evans, G.
535 J.: Quantification of aerosol chemical composition using continuous single particle
536 measurements, Atmos. Chem. Phys., 11, 7027-7044, doi:10.5194/acp-11-7027-2011, 2011.
537 Kammermann, L., Gysel, M., Weingartner, E., Herich, H., Cziczo, D. J., Holst, T.,
538 Svenningsson, B., Arneth, A., and Baltensperger, U.: Subarctic atmospheric aerosol
539 composition: 3. Measured and modeled properties of cloud condensation nuclei, J. Geophys.
540 Res.-Atmos., 115, 288-303, doi:10.1029/2009jd012447, 2010.
541 Kamphus, M., Ettner-Mahl, M., Klimach, T., Drewnick, F., Keller, L., Cziczo, D. J.,
542 Mertes, S., Borrmann, S., and Curtius, J.: Chemical composition of ambient aerosol, ice
543 residues and cloud droplet residues in mixed-phase clouds: single particle analysis during the

Cloud and Aerosol Characterization Experiment (CLACE 6), Atmos. Chem. Phys., 10, 8077-8095, doi:10.5194/acp-10-8077-2010, 2010.

Khalizov, A. F., Zhang, R. Y., Zhang, D., Xue, H. X., Pagels, J., and McMurry, P. H.: Formation of highly hygroscopic soot aerosols upon internal mixing with sulfuric acid vapor, J. Geophys. Res.-Atmos., 114, 730-734, doi:10.1029/2008jd010595, 2009.

Lambe, A. T., Ahern, A. T., Wright, J. P., Croasdale, D. R., Davidovits, P., and Onasch, T. B.: Oxidative aging and cloud condensation nuclei activation of laboratory combustion soot, J. Aerosol Sci., 79, 31-39, 2015.

Lan, Z. J., Huang, X. F., Yu, K. Y., Sun, T. L., Zeng, L. W., and Hu, M.: Light absorption of black carbon aerosol and its enhancement by mixing state in an urban atmosphere in South China, Atmos. Environ., 69, 118-123, doi:10.1016/j.atmosenv.2012.12.009, 2013.

Li, L., Huang, Z. X., Dong, J. G., Li, M., Gao, W., Nian, H. Q., Fu, Z., Zhang, G. H., Bi, X. H., Cheng, P., and Zhou, Z.: Real time bipolar time-of-flight mass spectrometer for analyzing single aerosol particles, Intl. J. Mass. Spectrom., 303, 118-124, doi:10.1016/j.ijms.2011.01.017, 2011a.

Li, W. J., Li, P. R., Sun, G. D., Zhou, S. Z., Yuan, Q., and Wang, W. X.: Cloud residues and interstitial aerosols from non-precipitating clouds over an industrial and urban area in northern China, Atmos. Environ., 45, 2488-2495, doi:10.1016/j.atmosenv.2011.02.044, 2011b.

Li, W. J., Zhou, S. Z., Wang, X. F., Xu, Z., Yuan, C., Yu, Y. C., Zhang, Q. Z., and Wang, W. X.: Integrated evaluation of aerosols from regional brown hazes over northern China in winter: Concentrations, sources, transformation, and mixing states, J. Geophys. Res., 116, 1-11, doi:10.1029/2010jd015099, 2011c.

Lin, Q., Zhang, G., Peng, L., Bi, X., Wang, X., Brechtel, F. J., Li, M., Chen, D., Peng, P., Sheng, G., and Zhou, Z.: In situ chemical composition measurement of individual cloud residue particles at a mountain site, southern China, Atmos. Chem. Phys., 17, 8473-8488, doi:10.5194/acp-17-8473-2017, 2017.

570 Matsui, H.: Black carbon simulations using a size- and mixing-state-resolved
571 three-dimensional model: 2. Aging timescale and its impact over East Asia, J. Geophys.
572 Res.-Atmos., 121, 1808-1821, doi:10.1002/2015jd023999, 2016.
573 McFiggans, G., Artaxo, P., Baltensperger, U., Coe, H., Facchini, M. C., Feingold, G.,
574 Fuzzi, S., Gysel, M., Laaksonen, A., Lohmann, U., Mentel, T. F., Murphy, D. M., O'Dowd, C.
575 D., Snider, J. R., and Weingartner, E.: The effect of physical and chemical aerosol properties on
576 warm cloud droplet activation, Atmos. Chem. Phys., 6, 2593-2649, 2006.
577 Moffet, R. C., and Prather, K. A.: In-situ measurements of the mixing state and optical
578 properties of soot with implications for radiative forcing estimates, Proc. Natl. Acad. Sci. USA,
579 106, 11872-11877, doi:10.1073/pnas.0900040106, 2009.
580 Peng, J. F., Hu, M., Guo, S., Du, Z. F., Zheng, J., Shang, D. J., Zamora, M. L., Zeng, L. M.,
581 Shao, M., Wu, Y. S., Zheng, J., Wang, Y., Glen, C. R., Collins, D. R., Molina, M. J., and Zhang,
582 R. Y.: Markedly enhanced absorption and direct radiative forcing of black carbon under
583 polluted urban environments, Proc. Natl. Acad. Sci. USA, 113, 4266-4271,
584 doi:10.1073/pnas.1602310113, 2016.
585 Petzold, A., Ogren, J. A., Fiebig, M., Laj, P., Li, S. M., Baltensperger, U., Holzer-Popp, T.,
586 Kinne, S., Pappalardo, G., Sugimoto, N., Wehrli, C., Wiedensohler, A., and Zhang, X. Y.:
587 Recommendations for reporting "black carbon" measurements, Atmos. Chem. Phys., 13,
588 8365-8379, 2013.
589 Qin, X. Y., Bhave, P. V., and Prather, K. A.: Comparison of two methods for obtaining
590 quantitative mass concentrations from aerosol time-of-flight mass spectrometry measurements,
591 Anal. Chem., 78, 6169-6178, doi:10.1021/ac060395q, 2006.
592 Roth, A., Schneider, J., Klimach, T., Mertes, S., van Pinxteren, D., Herrmann, H., and
593 Borrmann, S.: Aerosol properties, source identification, and cloud processing in orographic
594 clouds measured by single particle mass spectrometry on a central European mountain site
595 during HCCT-2010, Atmos. Chem. Phys., 16, 505-524, doi:10.5194/acp-16-505-2016, 2016.
596 Schroder, J. C., Hanna, S. J., Modini, R. L., Corrigan, A. L., Kreidenwies, S. M.,
597 Macdonald, A. M., Noone, K. J., Russell, L. M., Leaitch, W. R., and Bertram, A. K.:

598 Size-resolved observations of refractory black carbon particles in cloud droplets at a marine
599 boundary layer site, Atmos. Chem. Phys., 15, 1367-1383, doi:10.5194/acp-15-1367-2015,
600 2015.
601 Sellegri, K., Laj, P., Dupuy, R., Legrand, M., Preunkert, S., and Putaud, J. P.:
602 Size-dependent scavenging efficiencies of multicomponent atmospheric aerosols in clouds, J.
603 Geophys. Res.-Atmos., 108, 651-663, 2003.
604 Shingler, T., Dey, S., Sorooshian, A., Brechtel, F. J., Wang, Z., Metcalf, A., Coggon, M.,
605 Mulmenstadt, J., Russell, L. M., Jonsson, H. H., and Seinfeld, J. H.: Characterisation and
606 airborne deployment of a new counterflow virtual impactor inlet, Atmos. Meas. Tech., 5,
607 1259-1269, doi:10.5194/amt-5-1259-2012, 2012.
608 Song, X. H., Hopke, P. K., Fergenson, D. P., and Prather, K. A.: Classification of single
609 particles analyzed by ATOFMS using an artificial neural network, ART-2A, Anal. Chem., 71,
610 860-865, 1999.
611 Sorooshian, A., Wang, Z., Coggon, M. M., Jonsson, H. H., and Ervens, B.: Observations
612 of Sharp Oxalate Reductions in Stratocumulus Clouds at Variable Altitudes: Organic Acid and
613 Metal Measurements During the 2011 E-PEACE Campaign, Environ. Sci. Technol., 47,
614 7747-7756, doi:10.1021/es4012383, 2013.
615 Straub, D. J., Hutchings, J. W., and Herckes, P.: Measurements of fog composition at a
616 rural site, Atmos. Environ., 47, 195-205, doi:10.1016/j.atmosenv.2011.11.014, 2012.
617 van Pinxteren, D., Fomba, K. W., Mertes, S., Muller, K., Spindler, G., Schneider, J., Lee,
618 T., Collett, J. L., and Herrmann, H.: Cloud water composition during HCCT-2010: Scavenging
619 efficiencies, solute concentrations, and droplet size dependence of inorganic ions and dissolved
620 organic carbon, Atmos. Chem. Phys., 16, 3185-3205, doi:10.5194/acp-16-3185-2016, 2016.
621 Wang, Z., Wang, T., Guo, J., Gao, R., Xue, L. K., Zhang, J. M., Zhou, Y., Zhou, X. H.,
622 Zhang, Q. Z., and Wang, W. X.: Formation of secondary organic carbon and cloud impact on
623 carbonaceous aerosols at Mount Tai, North China, Atmos. Environ., 46, 516-527,
624 doi:10.1016/j.atmosenv.2011.08.019, 2012.

Weingartner, E., Saathoff, H., Schnaiter, M., Streit, N., Bitnar, B., and Baltensperger, U.: Absorption of light by soot particles: determination of the absorption coefficient by means of aethalometers, J. Aerosol Sci., 34, 1445-1463, doi:http://dx.doi.org/10.1016/S0021-8502(03)00359-8, 2003.

Wenzel, R. J., Liu, D. Y., Edgerton, E. S., and Prather, K. A.: Aerosol time-of-flight mass spectrometry during the Atlanta Supersite Experiment: 2. Scaling procedures, J. Geophys. Res.-Atmos., 108, 447-457, doi:10.1029/2001jd001563, 2003.

Wu, D., Wu, C., Liao, B., Chen, H., Wu, M., Li, F., Tan, H., Deng, T., Li, H., Jiang, D., and Yu, J. Z.: Black carbon over the South China Sea and in various continental locations in South China, Atmos. Chem. Phys., 13, 12257-12270, doi:10.5194/acp-13-12257-2013, 2013.

Xing, J. H., Takahashi, K., Yabushita, A., Kinugawa, T., Nakayama, T., Matsumi, Y., Tonokura, K., Takami, A., Imamura, T., Sato, K., Kawasaki, M., Hikida, T., and Shimono, A.: Characterization of Aerosol Particles in the Tokyo Metropolitan Area using Two Different Particle Mass Spectrometers, Aerosol Sci. Tech., 45, 315-326, doi:10.1080/02786826.2010.533720, 2011.

Yu, H., Wu, C., Wu, D., and Yu, J. Z.: Size distributions of elemental carbon and its contribution to light extinction in urban and rural locations in the pearl river delta region, China, Atmos. Chem. Phys., 10, 5107-5119, doi:10.5194/acp-10-5107-2010, 2010.

Zaveri, R. A., Barnard, J. C., Easter, R. C., Riemer, N., and West, M.: Particle-resolved simulation of aerosol size, composition, mixing state, and the associated optical and cloud condensation nuclei activation properties in an evolving urban plume, J. Geophys. Res.-Atmos., 115, 1383-1392, doi:10.1029/2009jd013616, 2010.

Zelenyuk, A., Imre, D., Earle, M., Easter, R., Korolev, A., Leaitch, R., Liu, P., Macdonald, A. M., Ovchinnikov, M., and Strapp, W.: In Situ Characterization of Cloud Condensation Nuclei, Interstitial, and Background Particles Using the Single Particle Mass Spectrometer, SPLAT II, Anal. Chem., 82, 7943-7951, doi:10.1021/Ac1013892, 2010.

Zhang, G., Lin, Q., Peng, L., Yang, Y., Fu, Y., Bi, X., Li, M., Chen, D., Chen, J., Cai, Z., Wang, X., Peng, P., Sheng, G., and Zhou, Z.: Insight into the in-cloud formation of oxalate

653 based on in situ measurement by single particle mass spectrometry, Atmos. Chem. Phys.
654 Discuss., 2017, 1-39, doi:10.5194/acp-2017-763, 2017.
655 Zhang, G. H., Bi, X. H., Chan, L. Y., Li, L., Wang, X. M., Feng, J. L., Sheng, G. Y., Fu, J.
656 M., Li, M., and Zhou, Z.: Enhanced trimethylamine-containing particles during fog events
657 detected by single particle aerosol mass spectrometry in urban Guangzhou, China, Atmos.
658 Environ., 55, 121-126, doi:10.1016/j.atmosenv.2012.03.038, 2012.
659 Zhang, G. H., Bi, X. H., Chan, L. Y., Wang, X. M., Sheng, G. Y., and Fu, J. M.:
660 Size-segregated chemical characteristics of aerosol during haze in an urban area of the Pearl
661 River Delta region, China, Urban Climate, 4, 74-84, doi:10.1016/j.uclim.2013.05.002, 2013.
662 Zhang, G. H., Bi, X. H., He, J. J., Chen, D. H., Chan, L. Y., Xie, G. W., Wang, X. M.,
663 Sheng, G. Y., Fu, J. M., and Zhou, Z.: Variation of secondary coatings associated with
664 elemental carbon by single particle analysis, Atmos. Environ., 92, 162-170,
665 doi:10.1016/j.atmosenv.2014.04.018, 2014.
666 Zhou, Y., Wang, T., Gao, X. M., Xue, L. K., Wang, X. F., Wang, Z., Gao, J. A., Zhang, Q.
667 Z., and Wang, W. X.: Continuous observations of water-soluble ions in PM2.5 at Mount Tai
668 (1534 ma.s.l.) in central-eastern China, J. Atmos. Chem., 64, 107-127, 2009.
669 Zuberi, B., Johnson, K. S., Aleks, G. K., Molina, L. T., and Laskin, A.: Hydrophilic
670 properties of aged soot, Geophys. Res. Lett., 32, 67-106, doi:10.1029/2004gl021496, 2005.
671

672 **Figure captions**

673 Fig. 1. Temporal profiles (with a 1 hour resolution) of $PM_{2.5}$, EBC mass concentrations,
674 number of BC-containing particles by SPAMS, RH and visibility. Three cloud events are
675 illustrated with black bars above the figure. $PM_{2.5}$ during the cloud events corresponded to the
676 cloud INT particles. EBC and number of BC-containing particles data were shown for all
677 categories, including the cloud-free, cloud RES, and cloud INT particles. The cloud INT
678 particles were only measured during Cloud III.

679 Fig. 2. Box and whisker plots of (a) concentration of EBC and (b) number fraction of
680 BC-containing particles for each cloud event. In a box and whisker plot, the lower, median
681 and upper lines of the box denote the 25^{th}, 50^{th}, and 75^{th} percentiles, respectively, and the
682 lower and upper edges of the whisker denote the 10^{th} and 90^{th} percentiles, respectively.

683 Fig. 3. (a) Average mass spectrum of the cloud RES BC-containing particles, and (b) the
684 RPA ratios of ammonium, sulfate, nitrate, oxidized organic markers, and other organic
685 markers (i.e., m/z 27$[C_2H_3]^+$, -26$[CN]^-$, 37$[C_3H]^+$, 50$[C_4H_2]^+$, 51$[C_4H_3]^+$, 61$[C_5H]^+$, and
686 63$[C_5H_3]^+$) to BC (carbon ion clusters ($C_n^{+/-}$, $n \leq 5$)), and the RPAs of BC for the cloud RES
687 and INT particles, respectively. Error bars represent the standard deviation in the hourly
688 average RPA or the RPA ratios within a 95% confidence interval.

689 Fig. 4. Normalized SPAMS particle count (to average count) over the measured size
690 range for the cloud-free, cloud INT, and cloud RES BC-containing particles, respectively. The
691 data were averaged throughout the sampling period.

Fig. 5. (a) Number fraction of each BC particle type in the cloud-free, INT, and RES BC-containing particles, and (b) the number fraction of each BC particle type in the cloud RES BC-containing particles separated for the three cloud events.

Fig. 6. Size-resolved Nf_{scav} estimated for the BC-containing particles and all the detected particles. The Nf_{scav} is calculated as the ratio of the average number size distribution for the cloud RES particles to the sum of the average number size distributions for the cloud RES and INT particles. Errors were estimated assuming that the particle numbers detected by the SPAMS follow a Poisson distribution.

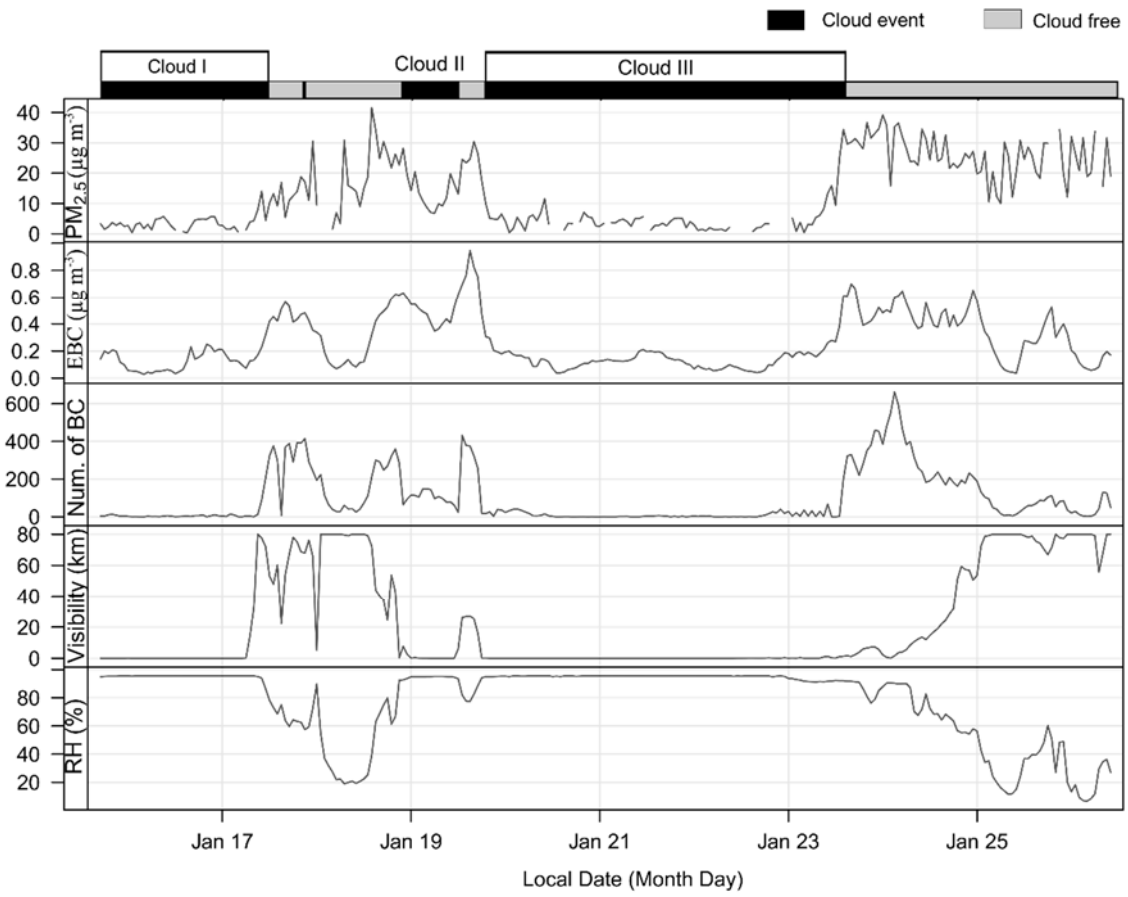
Cloud event
Cloud free
Cloud I
Cloud II
Cloud III
PM2.5 (μg m-3)
EBC (μg m-3)
Num. of BC
Visibility (km)
RH (%)
Jan 17
Jan 19
Jan 21
Jan 23
Jan 25
Local Date (Month Day)

Fig. 1.

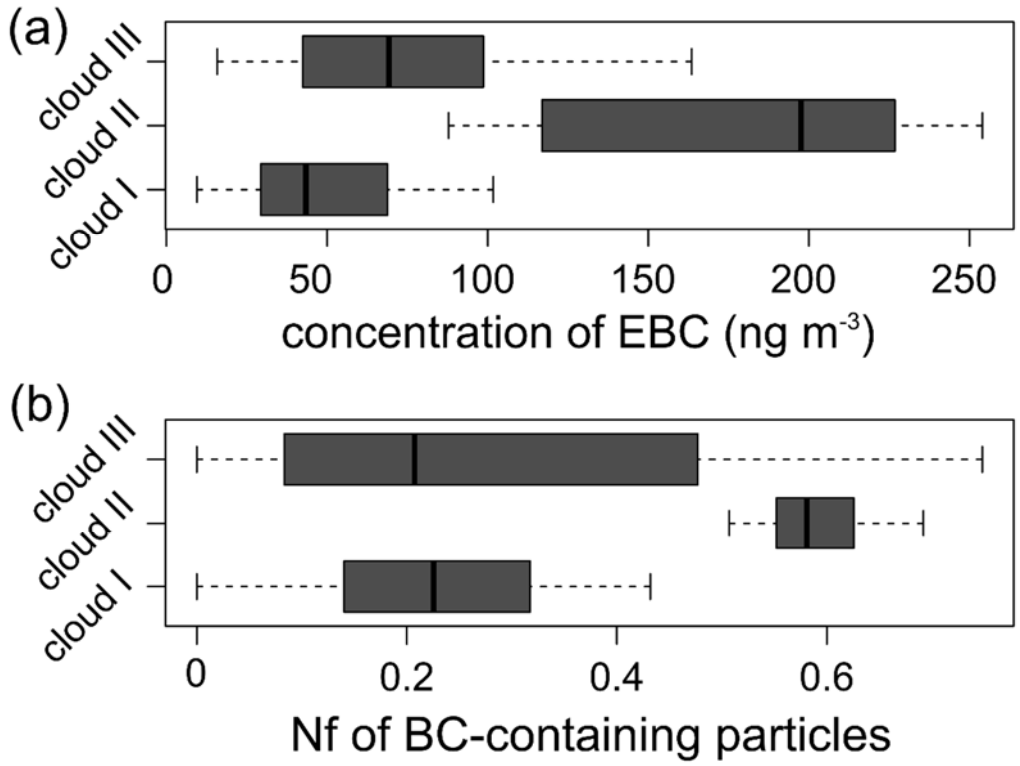
(a)
cloud III
cloud II
cloud I
0
50
100
150
200
250
concentration of EBC (ng m-3)
(b)
cloud III
cloud II
cloud I
0
0.2
0.4
0.6
Nf of BC-containing particles

702

703 Fig. 2.

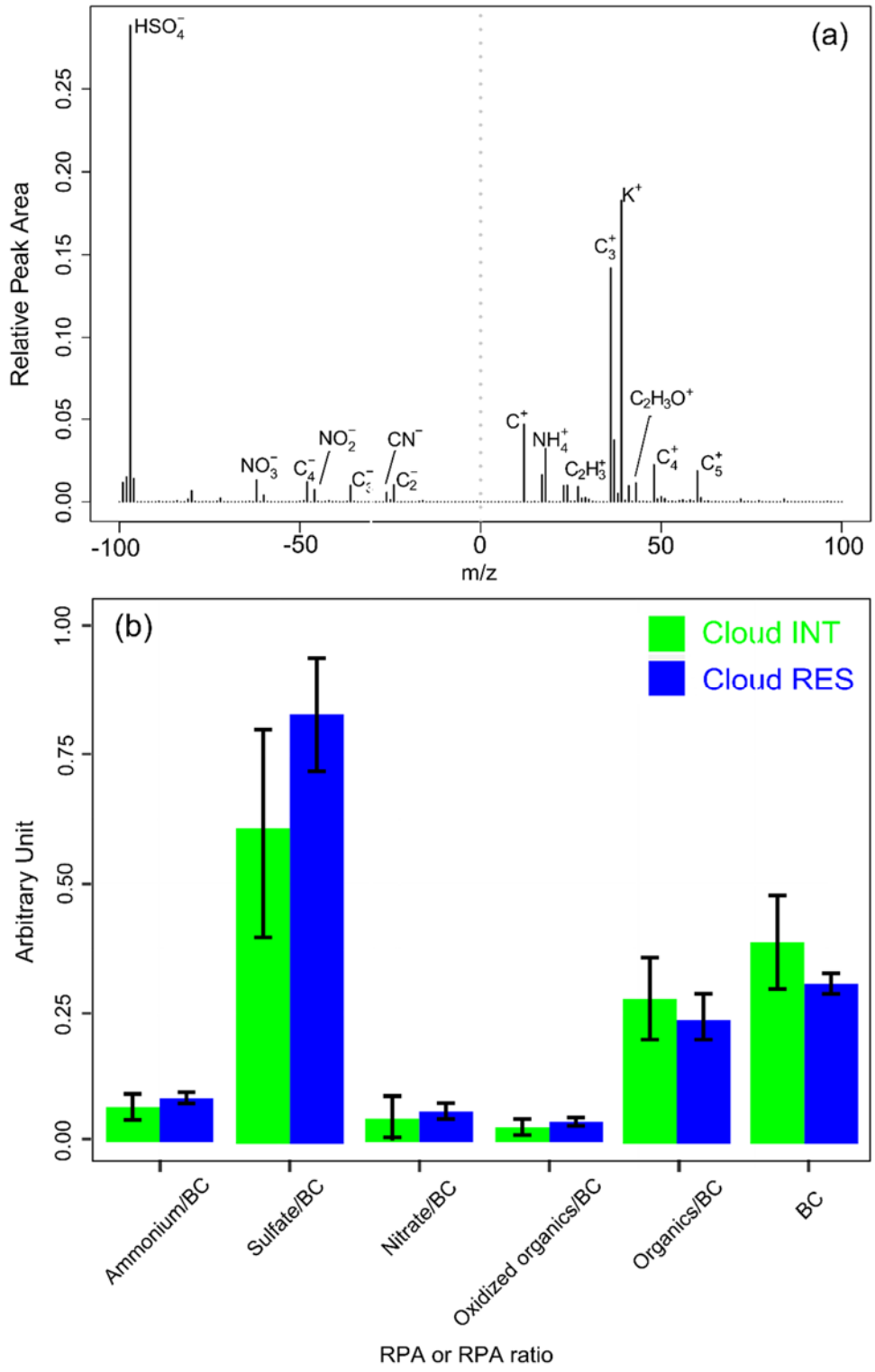
(a)
Relative Peak Area
0.00
0.05
0.10
0.15
0.20
0.25
HSO4−
NO3−
C4−
NO2−
C3−
CN−
C2−
C+
NH4+
C2H3+
C3+
K+
C2H3O+
C4+
C5+
-100
-50
0
50
100
m/z
(b)
Cloud INT
Cloud RES
Arbitrary Unit
0.00
0.25
0.50
0.75
1.00
Ammonium/BC
Sulfate/BC
Nitrate/BC
Oxidized organics/BC
Organics/BC
BC
RPA or RPA ratio

704

705 Fig. 3.

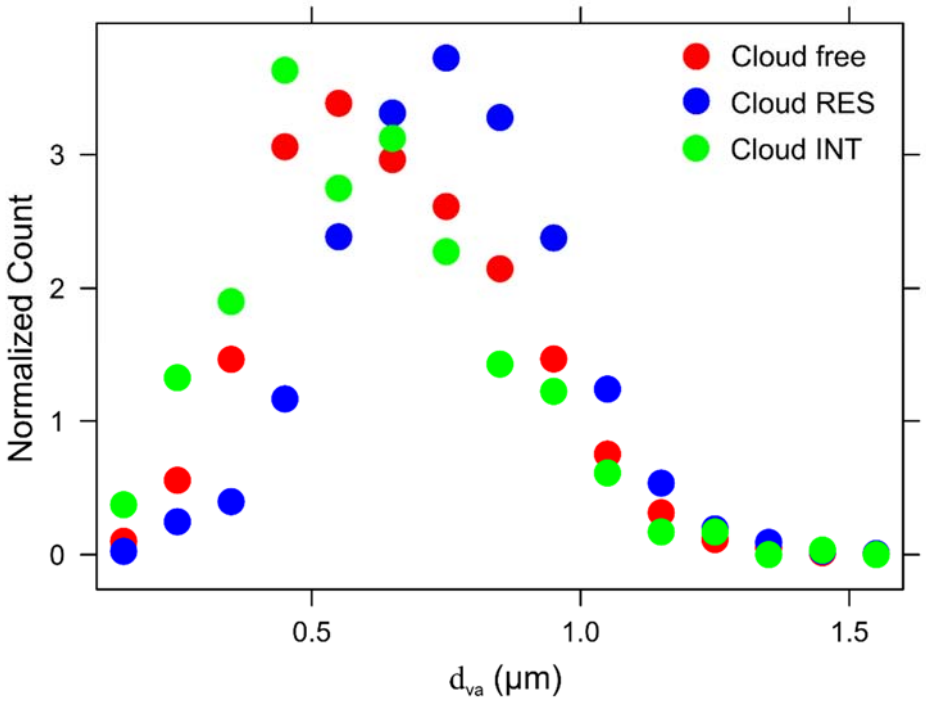
Cloud free
Cloud RES
Cloud INT
Normalized Count
0
1
2
3
0.5
1.0
1.5
d_{va} (μm)

706

707 **Fig. 4.**

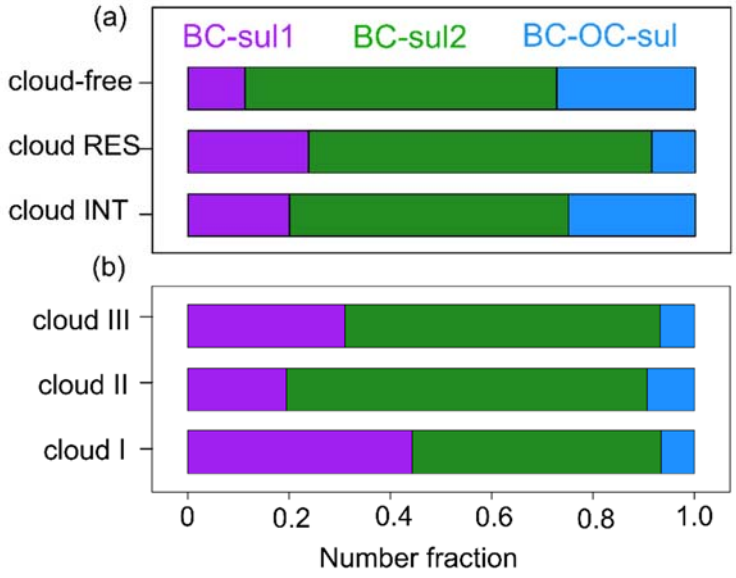
(a)
BC-sul1
BC-sul2
BC-OC-sul
cloud-free
cloud RES
cloud INT
(b)
cloud III
cloud II
cloud I
0
0.2
0.4
0.6
0.8
1.0
Number fraction

708

709 **Fig. 5.**

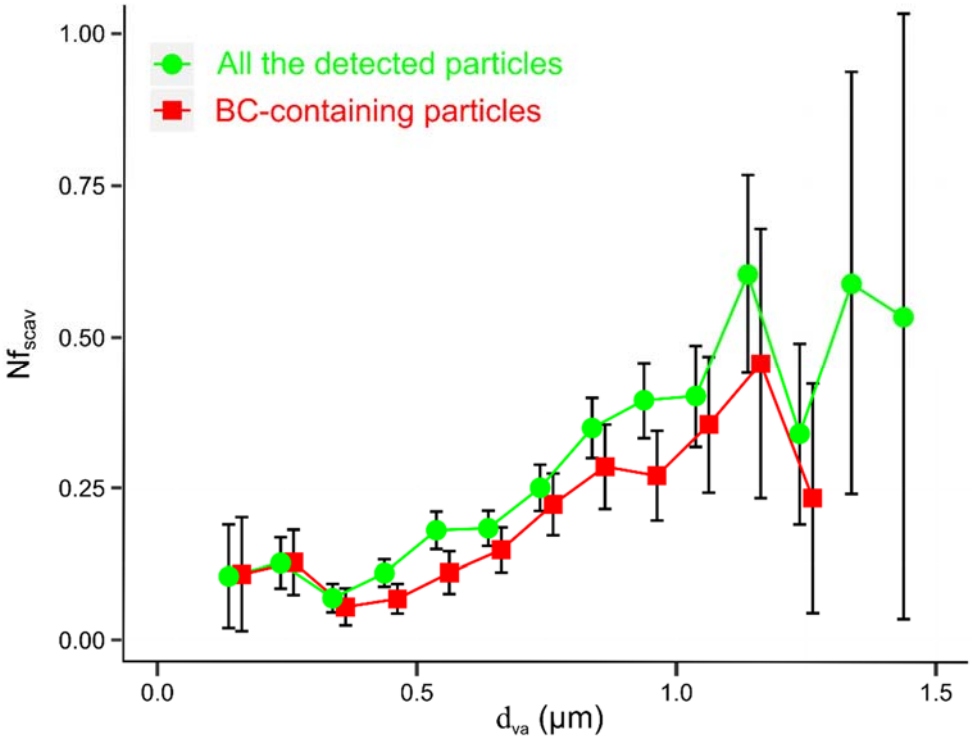
All the detected particles
BC-containing particles
1.00
0.75
0.50
0.25
0.00
Nf_{scav}
0.0
0.5
1.0
1.5
d_{va} (μm)

710

711 **Fig. 6.**

Supplement for

The single-particle mixing state and cloud scavenging of black carbon: a case study at a high-altitude mountain site in southern China

Guohua Zhang [1], Qinhao Lin [1, 2], Long Peng [1, 2], Xinhui Bi [1,*], Duohong Chen [3], Mei Li [4, 5], Lei Li [4, 5], Fred J. Brechtel [6], Jianxin Chen [7], Weijun Yan [7], Xinming Wang [1], Ping'an Peng [1], Guoying Sheng [1], Zhen Zhou [4, 5]

[1]State Key Laboratory of Organic Geochemistry and Guangdong Key Laboratory of Environmental Resources Utilization and Protection, Guangzhou Institute of Geochemistry, Chinese Academy of Sciences, Guangzhou 510640, PR China

[2] Graduate University of Chinese Academy of Sciences, Beijing 100039, PR China

[3] State Environmental Protection Key Laboratory of Regional Air Quality Monitoring, Guangdong Environmental Monitoring Center, Guangzhou 510308, PR China

[4] Institute of Mass Spectrometer and Atmospheric Environment, Jinan University, Guangzhou 510632, China

[5] Guangdong Provincial Engineering Research Center for on-line source apportionment system of air pollution, Guangzhou 510632, China

[6] Brechtel Manufacturing Inc., Hayward, 94544, California, USA

[7] Shaoguan Environmental Monitoring Center, Shaoguan 512026, PR China

Correspondence should be addressed to Xinhui Bi (bixh@gig.ac.cn)

SPAMS

Individual particles are introduced into SPAMS through a critical orifice. They are focused and accelerated to specific velocities, determined by two continuous diode Nd:YAG laser beams (532 nm), which are used to trigger a pulsed laser (266 nm) to desorp/ionize the particles. The produced positive and negative molecular fragments are recorded. In summary, a velocity, a detection moment, and an ion mass spectrum are recorded for each ionized particle, while there is no mass spectrum for not ionized particles. The velocity could be converted to d_{va} based on a calibration using polystyrene latex spheres (PSL, Duke Scientific Corp., Palo Alto) with predefined sizes. The accuracy for the derived d_{va} is within ±10%.

Aethalometer data analysis

The absorption coefficients at seven different wavelengths (370, 450, 520, 590, 660, 880 and 950 nm) were obtained by the Aethalometers. A variable attenuation (ATN), is defined to represent the filter attenuation through the sample spot on a filter (Weingartner et al., 2003; Arnott et al., 2005; Backman et al., 2016). It is well known that the measured ATN may differ from the true aerosol absorption due to 'filter loading effect', a phenomenon which appears as a gradual decrease of instrumental response as the aerosol loading on the filter increases (Arnott et al., 2005). Therefore, two calibration factors are introduced to convert aethalometer attenuation measurements to "real" absorption coefficient (Weingartner et al., 2003). At 880 nm wavelength, light absorption can be attributed to BC alone rather than the other aerosol particles due to their significantly less absorption at long wavelength (e.g., Sandradewi et al., 2008; Yang et al., 2009). For AE–31, a specific attenuation cross-section σ_{ATN} of 16.6 m^2 g^{-1}, recommended by the manufacturer, was applied to calculate the EBC concentration with the equation: EBC = b_{ATN}/σ_{ATN}, where b_{ATN} is the optical attenuation coefficient. For AE-33, the ATN was converted to an EBC concentration using the mass absorption cross section of 7.77 m^2 g^{-1} according to the method recommended by Drinovec et al. (2015).

The AE-31 used in the present study may suffer from the effects described above. Differently, the AE-33 has been improved by the incorporation of a filter loading correction part, based on a two parallel spot measurement of optical absorption. It could provide a real-time output of the "loading compensation" parameter to compensate for the "loading effect". The details of the principle of operation, data deduction, and error budget of the AE-33, the inherent uncertainties in its technique and the corrections are extensively available in the literature (Drinovec et al., 2015). Therefore, we reported EBC concentration from the results of AE-33. The detection limit for EBC measurements is < 10 ng m^{-3} with uncertainty at ~2 ng m^{-3} at the time-base of 1 minute (http://www.mageesci.com/). As noted in the manuscript and Fig. S10, the EBC measured by AE-31 is significantly correlated (R^2 = 0.9, $p < 0.001$) with that measured by AE-33. Therefore, EBC concentrations derived from AE-31 were not corrected for the calculation of $Mf_{scav,EBC}$.

As shown in Fig. S10, AE-31 might underestimate ~15% of EBC for cloud INT particles in the calculation of $Mf_{scav,EBC}$. It is also noted that a threshold of 8 μm might underestimate the mass concentration of cloud RES EBC, since the size of droplets might extend to as low as 3 μm. Unfortunately, the size distribution of cloud droplets was not available for our study. Therefore, we assumed that the largest underestimate of the cloud RES particles is 30% to assess the uncertainties for $Mf_{scav,EBC}$ calculation. The mean $Mf_{scav,EBC}$ was recalculated to be 30-36%, when the assumed largest underestimate (i.e., 30%) of the cloud RES particles and ~15% underestimate of the cloud INT BC were taken into account in R1. Compared to mean $Mf_{scav,EBC}$ = 33%, the overall uncertainties for the estimate of mean $Mf_{scav,EBC}$ is with 10%.

69 Table S1. Average mass concentrations, mass fractions relative to fine particles and scavenged fractions of BC from the literatures.

Site	site type	season (year)	ave (± std) ($\mu g\ m^{-3}$)	mass fraction	$Mf_{scav,EBC}$ (%)	References
Shenzhen, Southern China	urban	Summer (2011)	4.0 ± 3.1	~11%	-[a]	(Lan, et al., 2013)
Guangzhou, Southern China	urban	Summer (2008)	8.86	-	-	(Wu, et al., 2013)
Guangzhou, Southern China	urban	Fall(2010)	4.3	~4%[b]	-	(Zhang, et al., 2013)
Shenzhen, Southern China	urban	Fall(2009)	6.0 ± 6.3	-	-	(Huang, et al., 2012)
Guangzhou, Southern China	Rural	Summer (2008)	2.62	-	-	(Wu, et al., 2013)
Ba Guang village, southern China	Rural	Fall(2009)	2.6 ± 1.0	-	-	(Huang, et al., 2012)
Mt. Soledad (251 m m.s.l.)	marine	Summer (2012)	0.07	-	-	(Schroder, et al., 2015)
Yongxing Island, Southern China	marine	Summer (2008)	0.54	-	-	(Wu, et al., 2013)
A coastal Chilean hill, (Valparaíso), 450 m a.s.l.	low-altitude	Winter (2013)	0.34 - 0.95	-	13 - 50	(Hitzenberger et al., 2016)
Puy de Dome (France), 1465 m a.s.l.	mid-altitude	Winter-spring (2001)	-	-	33 - 74	(Sellegri et al., 2003)
Nova Scotia, Canada (Below 1 km)	mid-altitude	Summer (1993)	0.06 ± 0.01	-	2 - 32	(Chylek et al., 1996)

Nova Scotia, Canada (1-3 km)	mid-high-altitude	Summer (1993)	0.22 ± 0.03	-	-	(Chylek et al., 1996)
Mt. Rax (1644 m a.s.l.)	high-altitude	Spring (1999)	0.43	-	-	(Hitzenberger et al., 2001)
Mt. Rax (1644 m a.s.l.)	high-altitude	Spring (2000)	0.72	-	54 ± 25	(Hitzenberger et al., 2001)
Alpine Jungfraujoch (Switzerland), 3850 m a.s.l.	high-altitude	Summer (2004)	0.06	-	61	(*Cozic et al.*, 2007)
Alpine Jungfraujoch (Switzerland), 3850 m a.s.l.	high-altitude	Winter (2004)	0.05	-	-	(*Cozic et al.*, 2007)

[a] not available.

[b] mass fraction relative to PM_3.

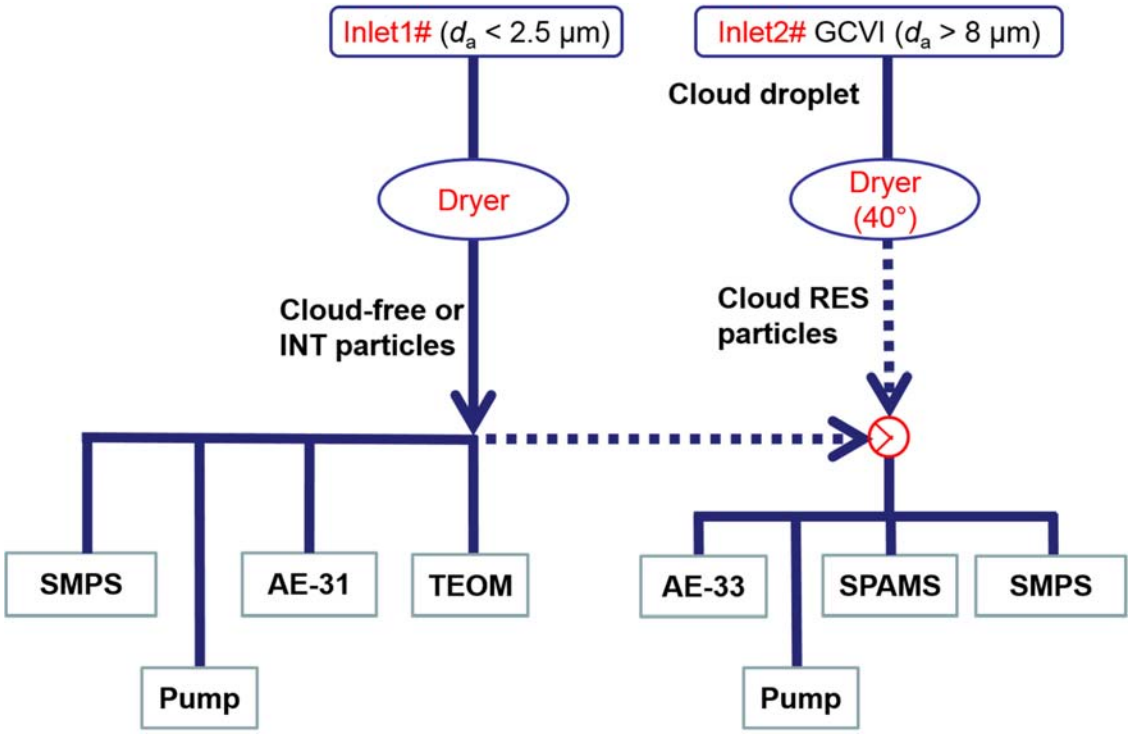

Figure S1. A scheme of the instrumentation setup in this study. The dash line illustrates that the sampling pipe was either connected to Inlet 1# or Inlet 2#. As described in section 2.1, the cloud INT and RES particles were intermittently measured by these instruments during Cloud III, through manually connect the sampling pipe to either Inlet 1# or Inlet 2# at approximately one-hour intervals. The GCVI includes various sensors to monitor the temperature/RH, visibility (http://belfortinstrument.com/products/all-environment-visibility-sensor/), and rainfall/snow (http://www.meltyourice.com/products/controllers/ds-82/). The integrated rainfall/snow sensor helps to exclude sampling during rainy periods. TEOM (https://www.thermofisher.com) measures the mass concentration of aerosol with the detection limited of ~100 ng m^{-3}, with an accuracy of ±0.75%. MSP SMPS (https://www.mspcorp.com) measures the number-based size distribution of particles

ranged between 10-1000 nm in 48 size bins, with a detection limit of ~1 cm^{-3}, and an accuracy of ±10%. Grimm SMPS (https://www.mspcorp.com) can measure the number-based size distribution of particles ranged between 10-1100 nm in 44 size bins, with a detection limit of ~1 cm^{-3}, and an accuracy of ±5%.

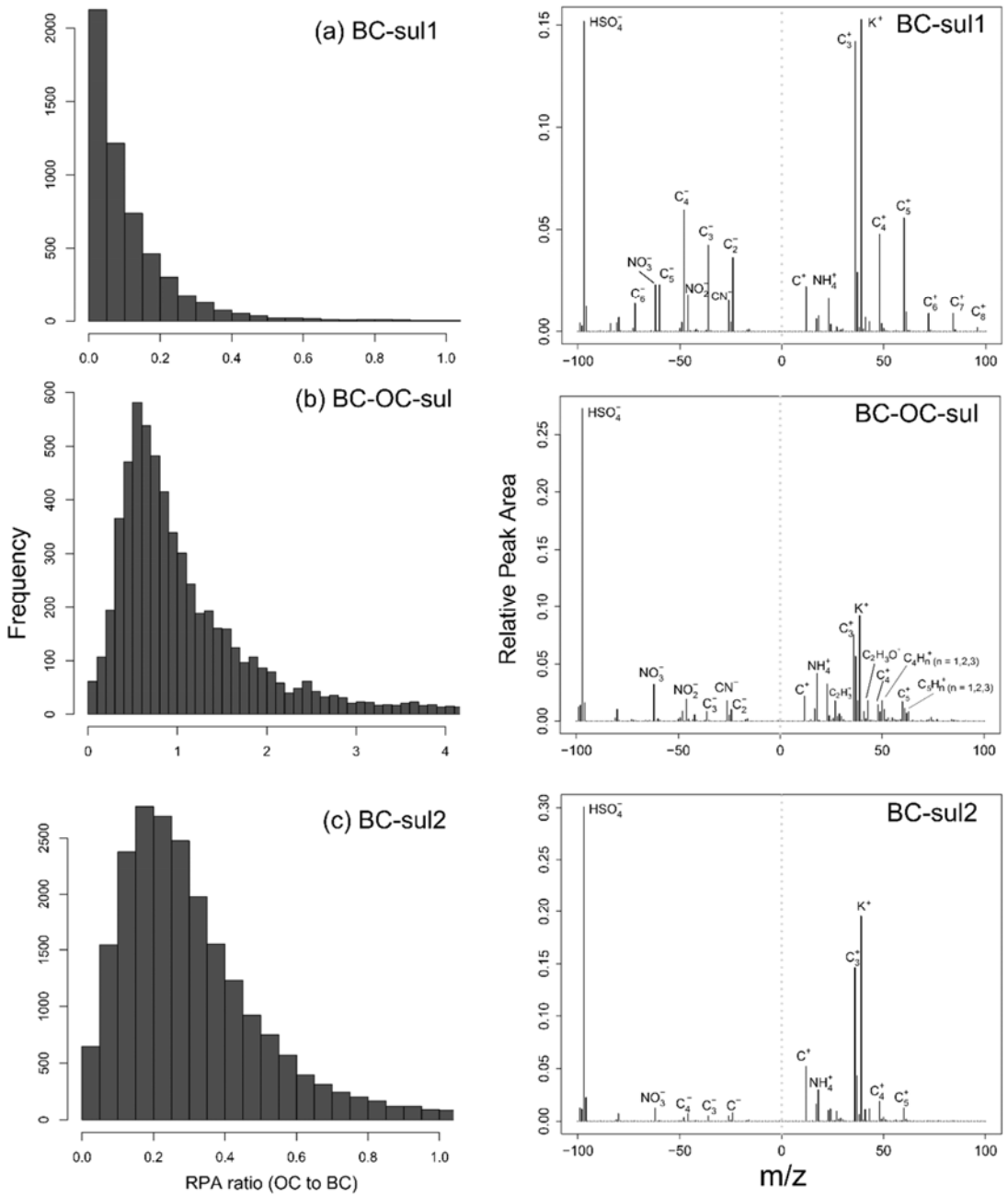

90

91 **Figure S2.** Statistic analysis on the RPA ratio of OC to BC (left), and the average mass

92 spectra (right) for the BC types. Markers were selected as m/z 27, 43, 50, 51, 61, 63, -26

93 for OC, and carbon ion clusters ($C_n^{+/-}$, $n \leq 5$) for BC, the same as those in Fig. 3. More

94 intense sulfate (RPA = ~0.3) was found for BC-sul2 and BC-OC-sul, relative to that

(RPA = ~0.15) for BC-sul1 type. More abundance of OC was found for BC-OC-sul, the mean peak area ratio OC/BC of which is ~1, higher than those (< 0.3) for other BC types.

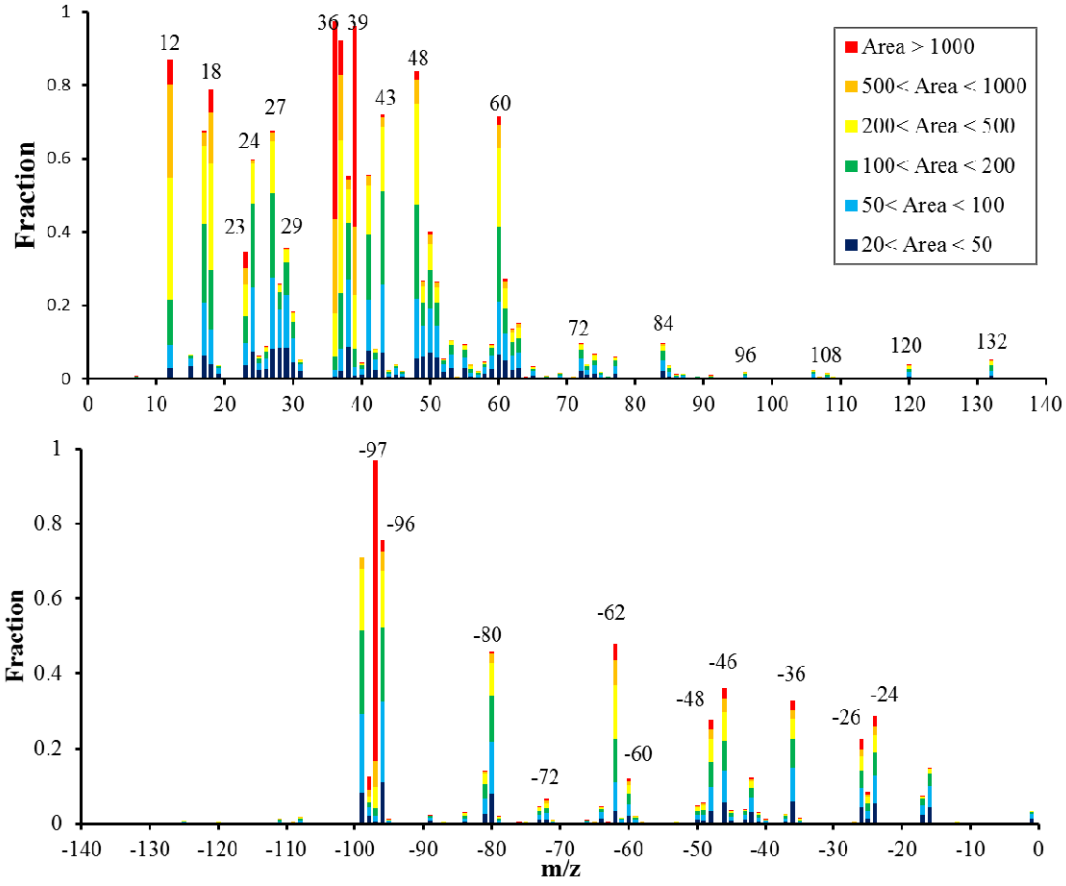

Figure S3. The number-based digitized mass spectrum of cloud-free BC-containing particles at the remote high-altitude site. Y-axis indicates the number fraction of total particles that had detectable amounts of these individual ion peaks.

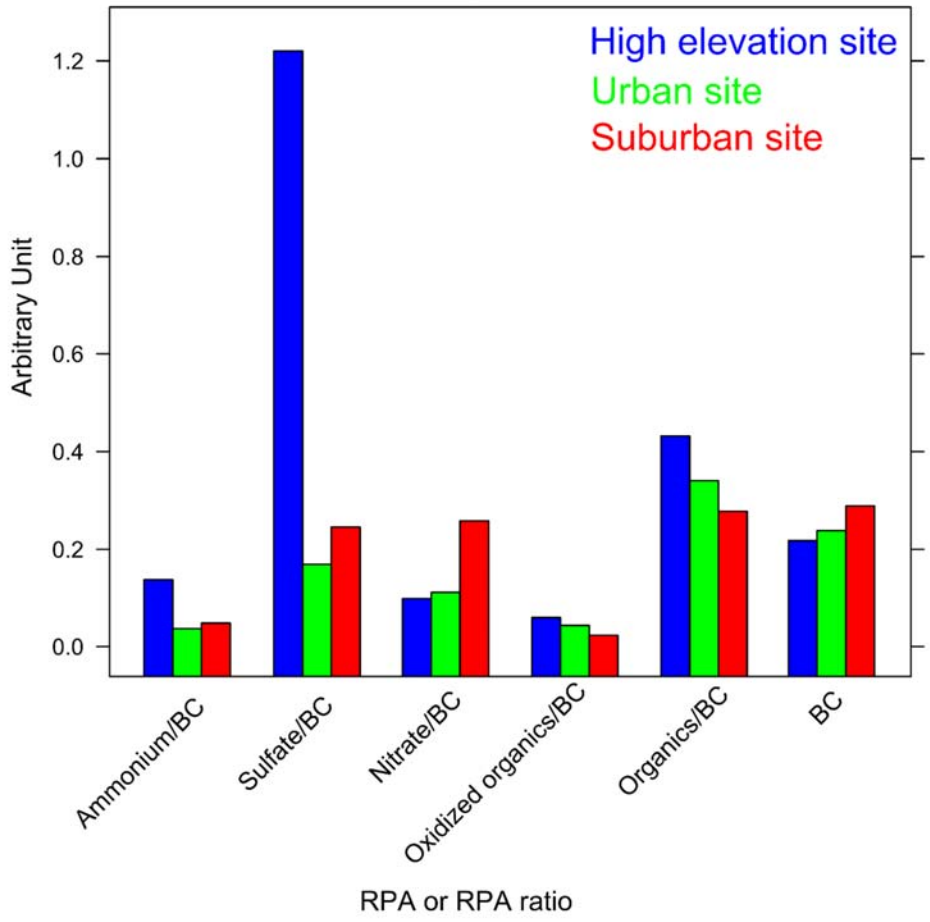

101

102 Figure S4. RPA ratio of ammonium (m/z 18), sulfate (m/z -97), nitrate (m/z -62),
103 oxidized organics (m/z 43), and other organics (m/z 27, 50, 51, 61, 63, -26) to BC, and
104 RPA of BC (carbon ion clusters ($C_n^{+/-}$, $n \leq 5$)) at the high elevation site, urban
105 (Guangzhou), and suburban sites (Heshan) during winter in southern China. The particles
106 in Guangzhou and Heshan were similarly measured by SPAMS during winter. Despite of
107 matrix effects due to the laser desorption/ionization for SPAMS, advances have been
108 made in semi-quantifying individual chemical species, either through multivariate
109 analysis or by applying peak intensities for specific ions (e.g., Jeong et al., 2011; Xing et
110 al., 2011; Healy et al., 2013). RPA, defined as the peak area of each m/z divided by the

111 total dual ion mass spectral peak area, is related to the relative amount of a species on a
112 particle. Compared to absolute peak area, RPA was commonly applied because it is less
113 sensitive to the variability in ion intensities associated with particle-laser interactions. It
114 is also noted that matrix effects might be lower when calculation was performed for
115 similar particle type, i.e., BC-containing particles.

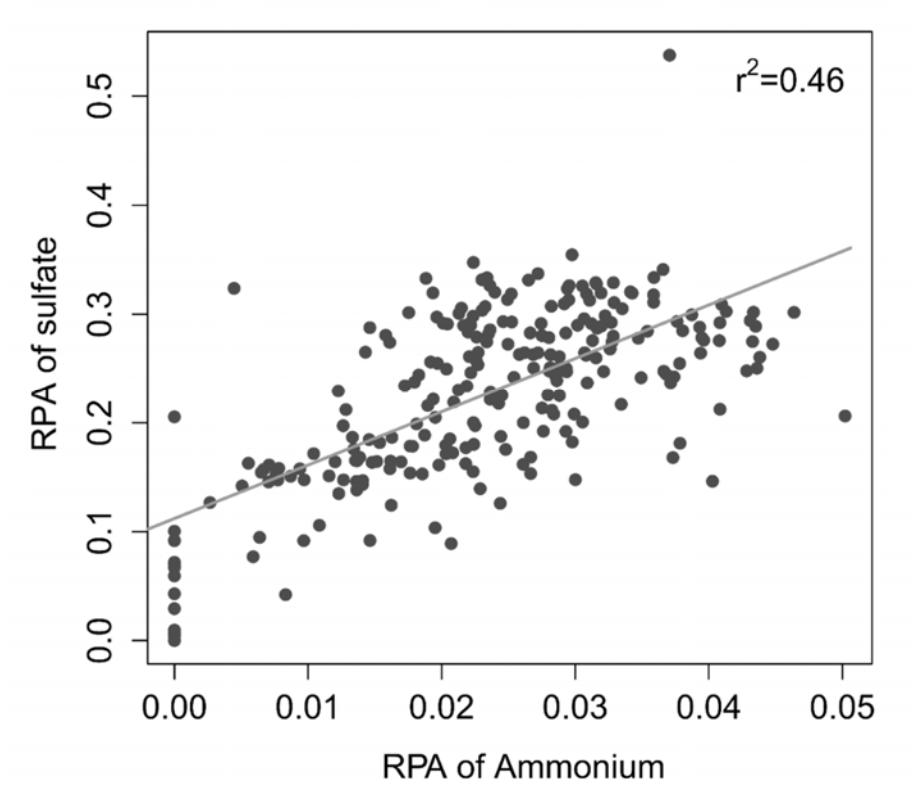

116

117 Figure S5. Correlation analysis of hourly average RPA for ammonium and sulfate
118 associated with BC-containing particles. The correlation coefficient is a bit lower than
119 expected might partly due to matrix effect in single particle mass spectrometry (e.g.,
120 Jeong et al., 2011; Xing et al., 2011; Healy et al., 2013).

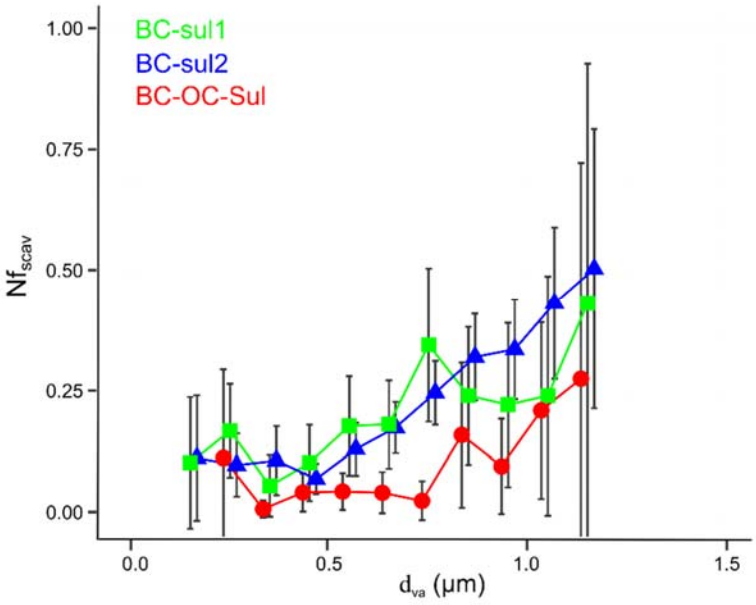

121

122 Figure S6. Size-resolved Nf_{act} estimated for three particle types of BC-containing
123 particles. Note that this data only collected during Cloud III event when both cloud RES
124 and INT particles were collected, however, not simultaneously but intermittently. It is
125 noted that although the Nf_{act} for BC-OC-sul type is lower than BC-sul types, the Nf_{act} for
126 all the BC-containing particles is similar to that of all the detected particles. We attributed
127 it to two reasons: (1) BC-OC-sul particles only accounted for ~20% of BC-containing
128 particles, and (2) the other particles also contained OC-dominated particles (~10%).

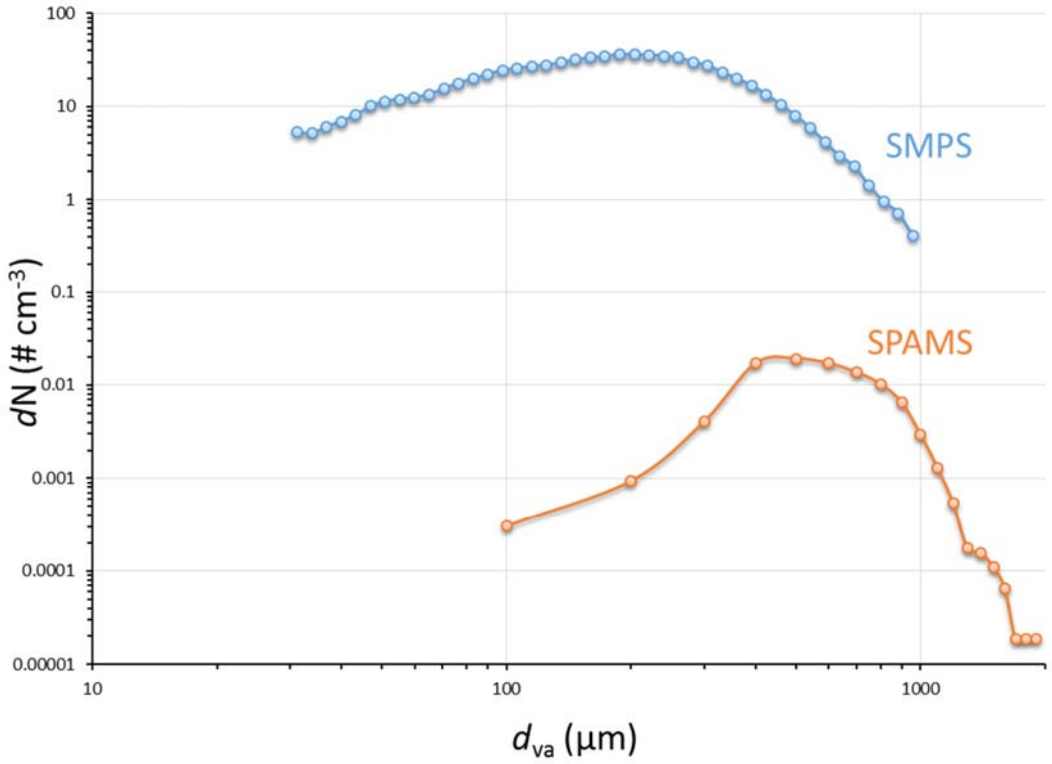

Figure S7. A representative comparison between the size distributions measured by the SPAMS and the SMPS within 12 hours measurements. It should be noted that the diameter is represented as d_{va} by SPAMS, while the diameter measured by the SMPS is represented as electrical mobility diameter (d_m). Herein, the d_m was first converted to the d_{va} for the comparison. The conversion could be simplified to $d_m = d_{va} * \rho_{eff}/\rho_0$ (DeCarlo et al., 2004), where ρ_{eff} refers to the effective density, ρ_0 is the unit density 1.0 g cm^{-3}. The ρ_{eff} is assumed to be 1.5 g cm^{-3} for the calculation (Hu et al., 2012).

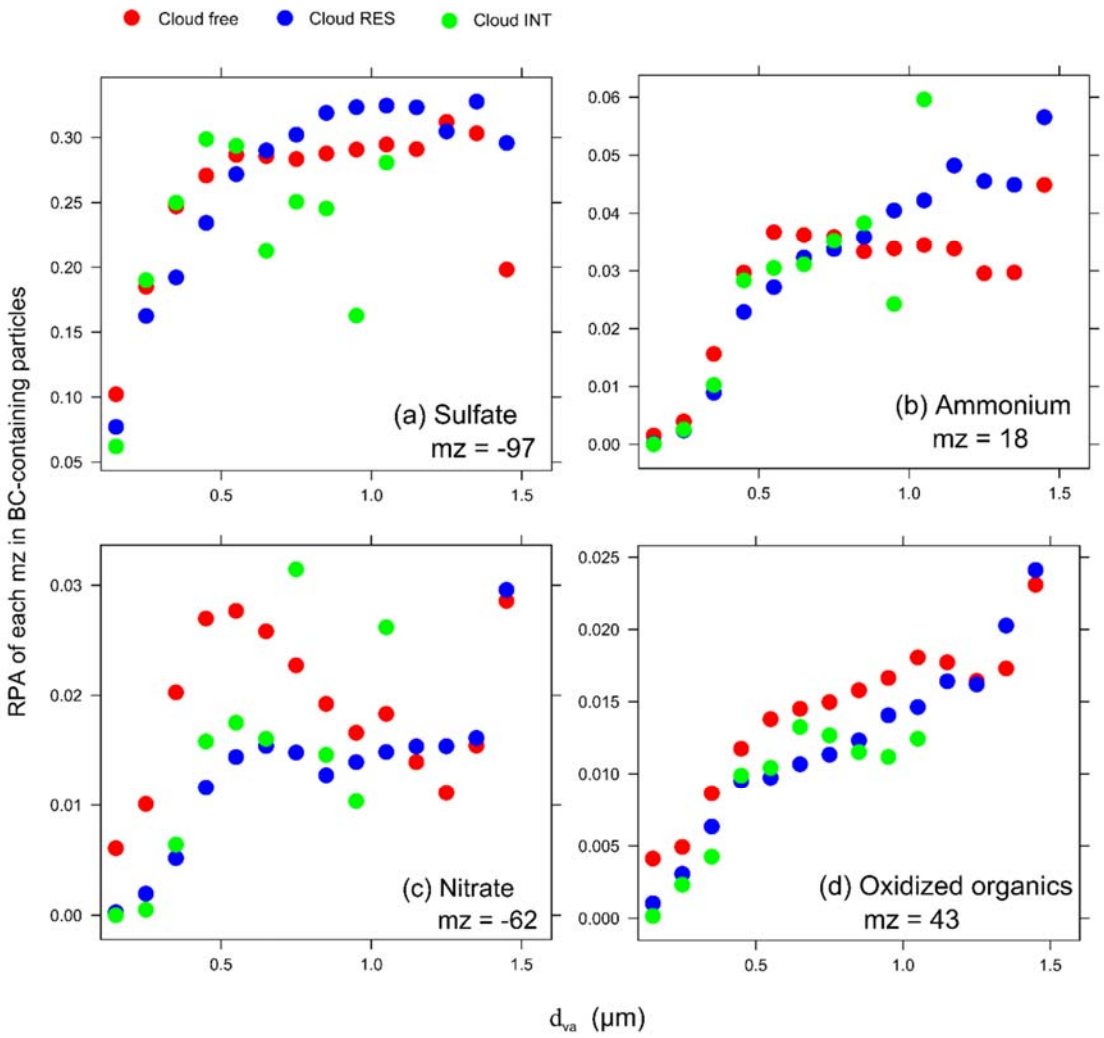

137

138 Figure S8. RPA of each secondary species associated with BC-containing particles in

139 cloud-free, INT, and RES particles as a function of particle sizes.

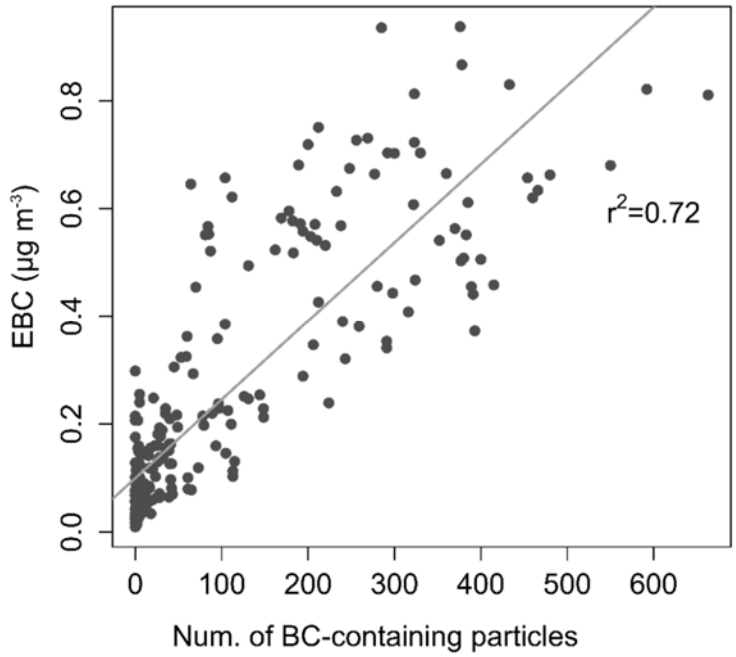

140

141 Figure S9. Correlation between time series of Num. of BC-containing particles and
142 concentration of EBC. The volume equivalent diameter of BC particles cores measured in
143 southern China was typically around 200 nm (Huang et al., 2011; Huang et al., 2012).
144 Huang et al. (2011) showed that a large fraction (> 60%) of BC particles are internally
145 mixed with a significant amount of non-refractory materials (coating thickness > 70 nm)
146 at a rural site in southern China. Furthermore, Yu et al. (2010) showed that over 50% of
147 BC are above 500 nm, also indicating internally mixed of BC, with regard that majority of
148 BC particles cores have volume equivalent diameter less than 500 nm (Huang et al., 2011;
149 Huang et al., 2012). As also discussed in section 3.1, BC-containing particles were already
150 heavily mixed with secondary species arriving at our site, and therefore they should be
151 larger enough for the detection by SPAMS.

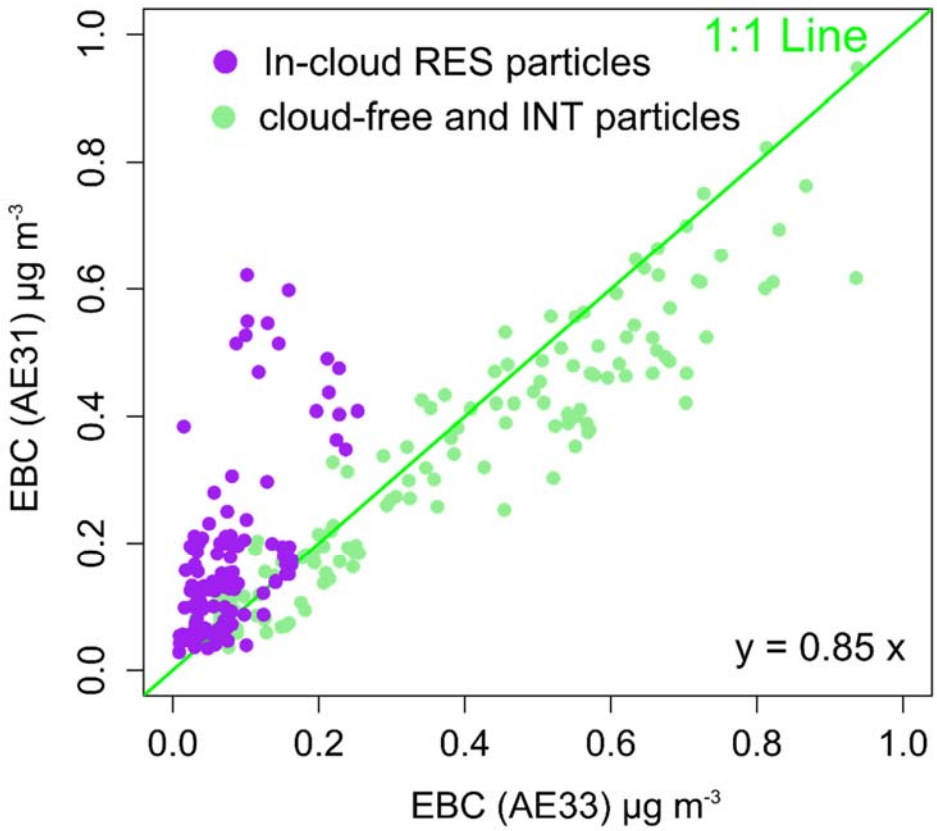

152

153 Figure S10. Correlation analysis of EBC measured by AE31 and AE33. They measured
154 the same aerosol for out-of-cloud (including cloud INT and cloud-free) particles. However,
155 during cloud events, AE33 measured cloud RES particles or cloud INT particles for some
156 periods, while AE31 measured cloud INT particles. Therefore, the EBC were compared
157 when the same aerosol were measured, as shown in green dots. The result indicates that
158 they are highly correlated, with EBC measured by AE31 only slightly lower than those by
159 AE33.

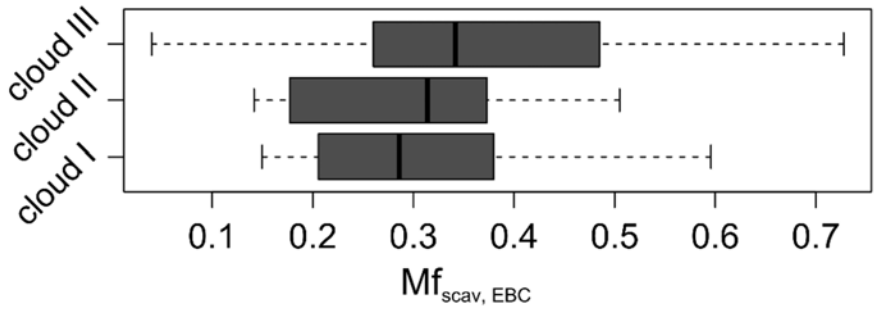

160

161 Figure S11. Box and whisker plot of $Mf_{scav,EBC}$ for each cloud event. In a box and whisker
162 plot, the lower, median and upper lines of the box denote the 25th, 50th, and 75th
163 percentiles, respectively, and the lower and upper edges of the whisker denote the 10th
164 and 90th percentiles, respectively.

165 Reference

166 Arnott, W. P., Hamasha, K., Moosmuller, H., Sheridan, P. J., and Ogren, J. A.: Towards
167 aerosol light-absorption measurements with a 7-wavelength Aethalometer:
168 Evaluation with a photoacoustic instrument and 3-wavelength nephelometer, Aerosol
169 Sci. Tech., 39, 17-29, doi:10.1080/027868290901972, 2005.
170 Backman, J., Schmeisser, L., Virkkula, A., Ogren, J. A., Asmi, E., Starkweather, S.,
171 Sharma, S., Eleftheriadis, K., Uttal, T., Jefferson, A., Bergin, M., and Makshtas, A.:
172 On Aethalometer measurement uncertainties and multiple scattering enhancement in
173 the Arctic, Atmos. Meas. Tech. Discuss., 2016, 1-31, doi:10.5194/amt-2016-294,
174 2016.
175 DeCarlo, P. F., Slowik, J. G., Worsnop, D. R., Davidovits, P., and Jimenez, J. L.: Particle
176 morphology and density characterization by combined mobility and aerodynamic
177 diameter measurements. Part 1: Theory, Aerosol Sci. Tech., 38, 1185-1205,
178 doi:10.1080/027868290903907, 2004.
179 Drinovec, L., Močnik, G., Zotter, P., Prévôt, A. S. H., Ruckstuhl, C., Coz, E., Rupakheti,
180 M., Sciare, J., Müller, T., Wiedensohler, A., and Hansen, A. D. A.: The "dual-spot"
181 Aethalometer: an improved measurement of aerosol black carbon with real-time
182 loading compensation, Atmos. Meas. Tech., 8, 1965-1979, doi:10.5194/amt-8-1965-
183 2015, 2015.
184 Healy, R. M., Sciare, J., Poulain, L., Crippa, M., Wiedensohler, A., Prevot, A. S. H.,
185 Baltensperger, U., Sarda-Esteve, R., McGuire, M. L., Jeong, C. H., McGillicuddy, E.,
186 O'Connor, I. P., Sodeau, J. R., Evans, G. J., and Wenger, J. C.: Quantitative
187 determination of carbonaceous particle mixing state in Paris using single-particle
188 mass spectrometer and aerosol mass spectrometer measurements, Atmos. Chem.
189 Phys., 13, 9479-9496, doi:10.5194/acp-13-9479-2013, 2013.
190 Huang, X. F., Gao, R. S., Schwarz, J. P., He, L. Y., Fahey, D. W., Watts, L. A.,
191 McComiskey, A., Cooper, O. R., Sun, T. L., Zeng, L. W., Hu, M., and Zhang, Y. H.:
192 Black carbon measurements in the Pearl River Delta region of China, J. Geophys.
193 Res., 116, 445-451, doi:10.1029/2010jd014933, 2011.
194 Huang, X. F., Sun, T. L., Zeng, L. W., Yu, G. H., and Luan, S. J.: Black carbon aerosol

195 characterization in a coastal city in South China using a single particle soot
196 photometer, Atmos. Environ., 51, 21-28, doi:10.1016/j.atmosenv.2012.01.056, 2012.
197 Jeong, C. H., McGuire, M. L., Godri, K. J., Slowik, J. G., Rehbein, P. J. G., and Evans, G.
198 J.: Quantification of aerosol chemical composition using continuous single particle
199 measurements, Atmos. Chem. Phys., 11, 7027-7044, doi:10.5194/acp-11-7027-2011,
200 2011.
201 Sandradewi, J., Prevot, A. S. H., Szidat, S., Perron, N., Alfarra, M. R., Lanz, V. A.,
202 Weingartner, E., and Baltensperger, U.: Using aerosol light absorption measurements
203 for the quantitative determination of wood burning and traffic emission contributions
204 to particulate matter, Environ. Sci. Technol., 42, 3316-3323, 2008.
205 Weingartner, E., Saathoff, H., Schnaiter, M., Streit, N., Bitnar, B., and Baltensperger, U.:
206 Absorption of light by soot particles: determination of the absorption coefficient by
207 means of aethalometers, J. Aerosol Sci., 34, 1445-1463,
208 doi:http://dx.doi.org/10.1016/S0021-8502(03)00359-8, 2003.
209 Xing, J. H., Takahashi, K., Yabushita, A., Kinugawa, T., Nakayama, T., Matsumi, Y.,
210 Tonokura, K., Takami, A., Imamura, T., Sato, K., Kawasaki, M., Hikida, T., and
211 Shimono, A.: Characterization of Aerosol Particles in the Tokyo Metropolitan Area
212 using Two Different Particle Mass Spectrometers, Aerosol Sci. Tech., 45, 315-326,
213 doi:10.1080/02786826.2010.533720, 2011.
214 Yang, M., Howell, S. G., Zhuang, J., and Huebert, B. J.: Attribution of aerosol light
215 absorption to black carbon, brown carbon, and dust in China - interpretations of
216 atmospheric measurements during EAST-AIRE, Atmos. Chem. Phys., 9, 2035-2050,
217 2009.
218 Yu, H., Wu, C., Wu, D., and Yu, J. Z.: Size distributions of elemental carbon and its
219 contribution to light extinction in urban and rural locations in the pearl river delta
220 region, China, Atmos. Chem. Phys., 10, 5107-5119, doi:10.5194/acp-10-5107-2010,
221 2010.